

IMPACT PARAMETER DEPENDENCE
OF K-VACANCY PRODUCTION IN
COPPER-NICKEL COLLISIONS AT 50 AND 65.6 MeV

by

CLARENCE HOWARD ANNETT
B.S., Texas A & M University, 1975

A MASTER'S THESIS

submitted in partial fulfillment of the
requirements for the degree

MASTER OF SCIENCE

Department of Physics
KANSAS STATE UNIVERSITY
Manhattan, Kansas

1977

Approved by:

C. A. Coche

Major Professor

Document
LD
2668
T4
1977
A55
C.2

206

TABLE OF CONTENTS

	<u>Page</u>
DEDICATION	11
ACKNOWLEDGMENTS	111
LIST OF FIGURES	1v
I. INTRODUCTION	1
II. THEORETICAL FOUNDATIONS	8
III. EXPERIMENTAL METHOD AND DATA	16
IV. SOLID TARGET EFFECTS AND CORRECTIONS TO DATA	37
V. MODIFICATIONS TO THEORY AND CONCLUSION	50
REFERENCES	55
APPENDIX A - Impact-Parameter Computer Code	
APPENDIX B - Coupled-Channel Computer Code	
APPENDIX C - Conversion of X-ray Production Probability to K-Vacancy Production Probability	
ABSTRACT	

DEDICATION

It is an honor and a pleasure for me to dedicate this thesis to Dr. Gilbert N. Plass, Chairman of the Physics Department, Texas A & M University, and the greatest physicist I have ever known. The memory of my association with him has been a continual source of inspiration throughout the preparation of this work, and continues to be a model for my professional career. I have tried to prepare this thesis in a way that would make him proud.

ACKNOWLEDGMENTS

I wish to extend particular thanks to my advisor, Dr. C. L. Cocke, for his encouragement and invaluable assistance with my research. I also wish to thank the members of my committee, Dr. Nate Folland and Dr. Patrick Richard.

For their invaluable assistance in taking the data, special thanks is due Dr. Basil Curnutte, Tom Bratton, Dr. S. L. Varghese, Steve Batsell, and Steve Spencer. The many long all-night runs necessary for the completion of this work would not have been possible without their help.

No words can adequately express my gratitude to my parents for their constant encouragement and inspiration throughout this trying time in my life. I also owe a major debt to Dr. Carl Rosenkilde, graduate student advisor, for many enlightening and productive discussions on matters not related to this thesis. Special thanks is due Dr. E. Brock Dale for his assistance with the electron microscope.

Continued financial support in the form of a teaching assistantship and a research assistantship from the Department of Physics, Kansas State University, is acknowledged and appreciated. The research project itself was funded by the U.S. Energy Research and Development Administration.

Finally, I will always be grateful to Reba Snavelly for her fine typing of this thesis.

LIST OF FIGURES

- Figure 1 Correlation diagram of a molecular excitation model for a near-symmetric collision.
- Figure 2 Schematic diagram of the collision process.
- Figure 3 Diagram of the experimental apparatus.
- Figure 4 Block diagram of the coincidence electronics.
- Figure 5 Results of the screened-Coulomb impact parameter calculation.
- Figure 6 Typical coincidence TAC spectrum for 50 MeV run.
- Figure 7 Typical coincidence and singles x-ray spectra for 50 MeV runs.
- Figure 8 Nickel K x-ray production probability $P_x(b)$ vs. impact parameter b for 50 MeV.
- Figure 9 Nickel K x-ray production probability $P_x(b)$ vs. impact parameter b for 65.6 MeV.
- Figure 10 Plot of count rate vs. distance from beam center for scans through the copper beam at 50 MeV.
- Figure 11 Universal curve used to correct $P(b)$ vs. b data for small-angle scattering.
- Figure 12 Beam charge state fractions emerging from $5\mu\text{g}/\text{cm}^2$ carbon foil.
- Figure 13 Total x-ray yield vs. nickel foil thickness and nickel K x-ray production probability vs. nickel foil thickness at 50 MeV.
- Figure 14 Detail of the two regions of the $2P\sigma-2P\pi$ energy difference ΔE .

I. Introduction

The study of inner-shell ionization really began with the discovery of X rays by Wilhelm Conrad Roentgen in 1895. Not long thereafter, the characteristic X rays of many elements were discovered, measured, and partially described by existing theories. Before 1920, several experiments¹ had shown that heavy elements would emit characteristic X rays when bombarded by alpha particles from naturally-radioactive sources. Not until the 1930's were heavy ions used as the projectiles to create inner-shell ionization, when they became available as beams from the newly-developed particle accelerators. Only two major experiments,² both performed in the late 1930's, observed inner-shell ionization produced by heavy ions. Except for sporadic efforts, the experimental study of inner-shell ionization was not pursued further until the 1960's.

On the basis of early experiments, a model for inner-shell ionization was developed. This model, which was detailed in 1958 by Merzbacher and Lewis,³ was quite successful in describing the inner-shell ionization of a heavy target atom by a light, swift projectile. Except for minor corrections,⁴ the model remains essentially unchanged today. The model describes a direct Coulomb ionization mechanism, wherein a swift point charge Z_1 penetrates a hydrogenlike atom of nuclear charge Z_2 . The condition under which the model is useful is $Z_1 \ll Z_2$. However, as Z_1 becomes more nearly equal to Z_2 (a more symmetric collision), and/or the projectile ion has a smaller velocity, this simple model no longer gives correct quantitative results.

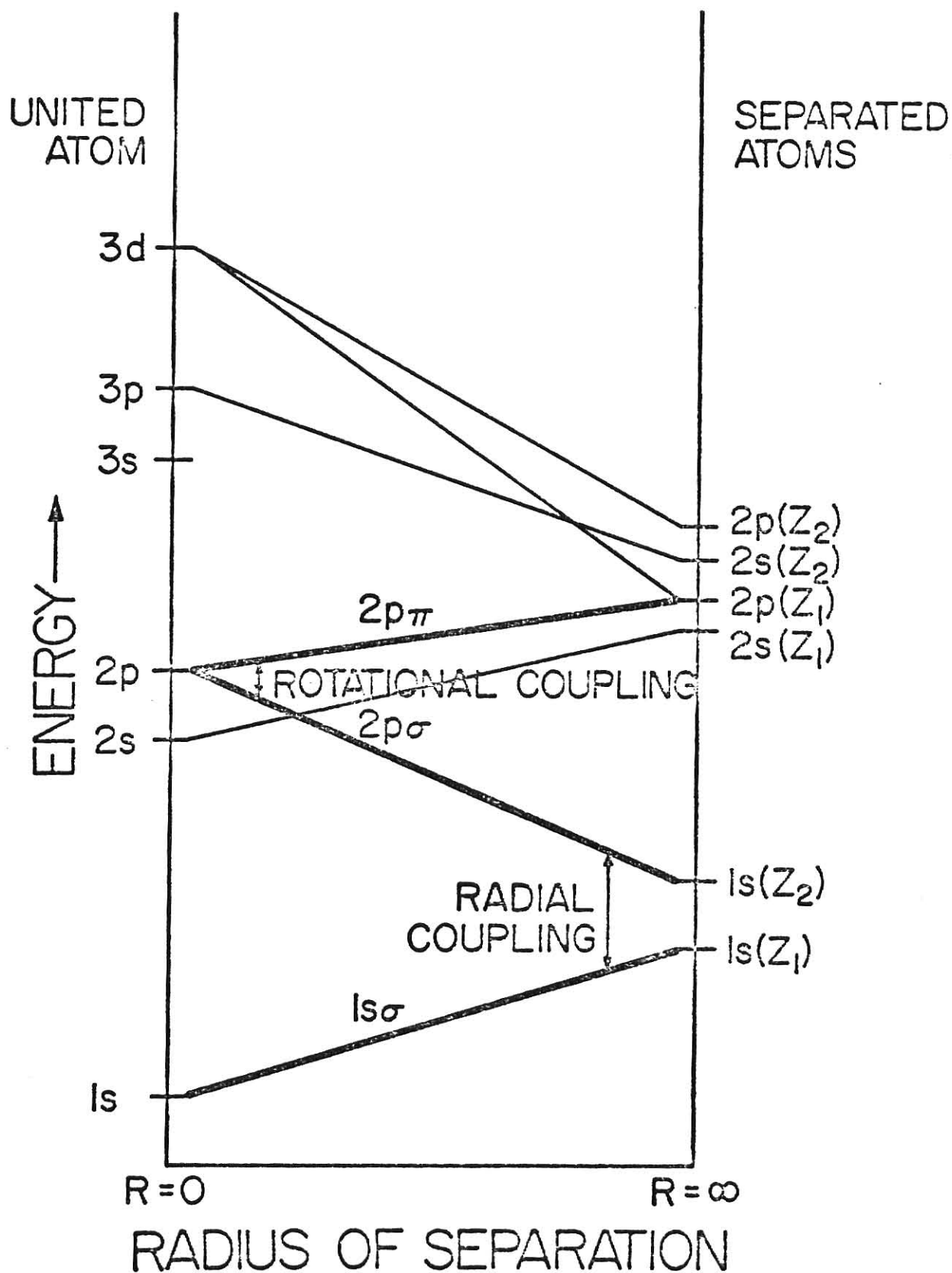
Experiments by Everhart and co-workers⁵ and by Fedorenko and co-workers⁶ on $\text{Ar} + \text{Ar}^+$ and $\text{Ne} + \text{Ne}^+$ systems in the early 1960's brought a renewed interest in the problem of inner-shell ionization in the regime where direct

Coulomb ionization is not valid. In particular, Everhart and Fedorenko observed very high vacancy production cross sections and a strong dependence of the differential cross section on the collision impact parameter. This new region of $Z_1/Z_2 \approx 1$ was subsequently explained by a different model. Often called the "electron promotion" or "molecular orbital" model, it was proposed by Fano and Lichten⁷ in a qualitative form. In recent years it has been quantified, expanded, and refined.^{8,9,10}

A schematic of the model is shown in Figure 1. This is called a correlation diagram, and is drawn for a collision of two atoms having atomic numbers Z_1 and Z_2 . For applicability to the following chapters, Z_1 is assumed to differ from Z_2 by only one unit, thus providing a near-symmetric collision. Z_1 is taken to be the heavier partner in the collision. On the right-hand side are plotted the energy levels of the separated atoms. On the left-hand side are plotted the energy levels of the united atom, and the lines connecting the two sets of energy levels show which levels correlate during the collision. The correlations are established by using Barat and Lichten's correlation rule,⁸ which states that the number of radial nodes in the wavefunction for each level must be conserved during the collision. Not all of the energy levels are shown, because only the lowest are considered important to the present experiment.

In this model, several processes exist by which k-vacancy production might occur. If there is a 2p vacancy in Z_1 , it becomes a 2p π vacancy in the united atom. At some small separation R, it may be transferred by rotational coupling to the 2p σ orbital, which ultimately correlates to the K-shell of Z_2 . It might further be transferred to the 1s σ orbital by radial coupling, thus removing a K-electron from Z_1 .

Figure 1. Partial schematic representation (correlation diagram) of a molecular excitation model for a near-symmetric collision where atomic numbers Z_1 and Z_2 differ by only one unit and $Z_1 > Z_2$.



If no 2p vacancies are brought into the collision by Z_1 , there are still several ways for producing K-vacancies. For instance, the vacancy might be produced by directly ionizing the 2p σ level. Such a vacancy could travel down via radial coupling to the 1s σ level. Or, an electron in the 1s σ level might be excited directly to the continuum with no intermediate steps. Alternately, other higher MO levels might be involved, making the process even more complex. However, these processes can be distinguished on theoretical grounds from the observed shape of the ionization probability versus impact parameter curve, and the signature for each process may be unique.

Also, ionization of the K-shell may proceed in this manner: During the collision, a vacancy is created in the 2p π correlated level at some nonzero separation R. As the atom and ion approach more closely, the vacancy is transferred down to the 2p σ level and an electron is transferred up to replace it. As the collision partners separate, the vacancy travels down, eventually leaving a K-vacancy in the 2p σ level of Z_2 . It may be transferred downward at some large separation distance to the 1s σ level, which results in removal of the K electron of Z_1 . The terms "rotational coupling" and "radial coupling" will be explained in the following chapter.

Thus, ionization of the K shell may be characterized as a multistep process for symmetric and near-symmetric ion-atom collisions. Noteworthy of this approach is that only a few electronic states are required to describe the process, since the assumption is made that the behavior of the outer-shell electrons does not affect the process significantly. This model has found particular applicability in studying the atomic interactions of heavy ions.

Collisions of this type, which result in ionization of the K shell of the target atom (Z_2), are easily observed either by detecting the X ray resulting from another electron cascading down to fill the K vacancy (if the fluorescence yield is large enough for this process to be favorable) or by detecting the Auger electrons resulting from the downward cascade. Thus, the signature of K-shell ionization is unique, whether it be the characteristic X ray (whose energy is well known) or the characteristic Auger electron of the target atom.

The research undertaken here involves a measurement of the impact-parameter dependent probability of K-shell ionization for a relatively high average Z system. The system under consideration is the near-symmetric collision of copper ($Z_1=29$) and nickel ($Z_2=28$) atoms, at moderate velocities relative to the K-shell electron velocity of nickel. A slightly asymmetric system is chosen because the target and projectile K-shell X rays can be distinguished easily. The probability of a vacancy ending up in the $2p\sigma$ level (the K-shell of nickel, $Z_2=28$) is deduced from the measurement. The results are compared with predictions of a molecular-excitation model,¹¹ with particular emphasis on the possible rotational coupling which takes place during the collision. (The radial coupling is largely ignored, since it is already well understood.^{12,13}) It should be noted that measuring an impact-parameter dependent probability for K-shell ionization is equivalent to measuring a differential cross section for K-vacancy production.

Although a standard impact-parameter ion-atom collision method¹⁴ may be used to arrive at a theoretical model, there is an easier method which will give the same result. This method will be reviewed in Section II.

Section III will detail the experiment and its results, while Section IV will consider solid-target effects and the resulting corrections to the data. Section V will present corrections to the theory and conclusions.

As a final introductory note, other methods of observing atomic collisions which produce K-vacancies have been used¹⁵ but will not be considered here. Much of the literature of heavy ion-atom collisions has been brought together in a recent review by Kessel and Fastrup,¹⁶ which contains an extensive list of useful references not directly applicable to this work.

II. Theoretical Foundations

In the collision to be considered in this thesis, the ratio $Z_1/Z_2 \approx 1$ and the collision is nearly symmetric. Thus, a direct Coulomb ionization model is no longer appropriate, and instead a molecular orbital (MO) model must be used to describe the collision. Much of the detailed mathematics may be found in Bates and Williams.¹⁷ However, it is possible to make an approximation which simplifies the calculation and has been shown to give good results. The development of Briggs and Macek⁹ is used for this presentation of the approximation.

The formalism is that of the perturbed stationary states (PSS) model, wherein the state of the evolving system is written as a linear combination of the molecular wavefunctions of the chosen basis. The complexity of such a calculation may be reduced by limiting the size of the set of basis states. Referring to Figure 1, the basis set for this work is chosen to consist of only two states--the $2p\sigma$ and $2p\pi$ molecular orbitals. This is called the independent-electron two-state approximation, and is used to calculate the impact-parameter dependent probability $P(b)$ for the transfer of a vacancy to the K shell through rotational coupling between the $2p\sigma$ and $2p\pi$ molecular orbitals. σ denotes a molecular state with an angular momentum quantum number (projected onto the internuclear axis) of zero; π denotes a molecular state with an angular momentum projection quantum number of one.

To derive the two-state coupled equations, we expand our system in terms of $\psi_1(r,R)$ and $\psi_2(r,R)$ where

$$H(R)\psi_1(r,R) = E_1\psi_1(r,R)$$

$$H(R)\psi_2(r,R) = E_2\psi_2(r,R) \quad (1)$$

and

$H(R)$ is the full Hamiltonian;

R is the internuclear radius, a function of time;

r is the radius of the target K electron;

$\psi_1(r,R)$ is the correct wavefunction for the $2p\sigma$ state;

$\psi_2(r,R)$ is the correct wavefunction for the $2p\pi$ state;

E_1 is the energy eigenvalue for the $2p\sigma$ state;

E_2 is the energy eigenvalue for the $2p\pi$ state.

We now write a molecular wavefunction with the proper phase factors:

$$\psi(t) = a_1\psi_1 e^{\frac{-i}{\hbar} \int_{-\infty}^t E_1 dt} + a_2\psi_2 e^{\frac{-i}{\hbar} \int_{-\infty}^t E_2 dt} \quad (2)$$

where t = time and a_1, a_2 are functions of time only.

This molecular wavefunction must satisfy the Schrodinger equation:

$$H(R)\psi = i\hbar \frac{d\psi}{dt} \quad (3)$$

Substituting (2) into (3), we obtain

$$\begin{aligned} a_1 E_1 \psi_1 e^{\frac{-i}{\hbar} \int_{-\infty}^t E_1 dt} + a_2 E_2 \psi_2 e^{\frac{-i}{\hbar} \int_{-\infty}^t E_2 dt} &= i\hbar \left(\dot{a}_1 \psi_1 + a_1 \frac{d\psi_1}{dt} - \frac{i}{\hbar} E_1 a_1 \psi_1 \right) e^{\frac{-i}{\hbar} \int_{-\infty}^t E_1 dt} \\ &+ i\hbar \left(\dot{a}_2 \psi_2 + a_2 \frac{d\psi_2}{dt} - \frac{i}{\hbar} E_2 a_2 \psi_2 \right) e^{\frac{-i}{\hbar} \int_{-\infty}^t E_2 dt} \end{aligned} \quad (4)$$

If we multiply (4) by ψ_1^* and integrate over all space, we obtain

$$\dot{a}_1 = a_2 \langle \psi_1 | \frac{\delta}{\delta t} | \psi_2 \rangle e^{\frac{-i}{\hbar} \int (E_2 - E_1) dt} + a_1 \langle \psi_1 | \frac{\delta}{\delta t} | \psi_1 \rangle \quad (5)$$

Similarly, multiplying (4) by ψ_2^* and integrating over all space, we obtain

$$\dot{a}_2 = a_1 \langle \psi_2 | \frac{\delta}{\delta t} | \psi_1 \rangle e^{\frac{+i}{\hbar} \int (E_2 - E_1) dt} + a_2 \langle \psi_2 | \frac{\delta}{\delta t} | \psi_2 \rangle \quad (6)$$

Now it is assumed that the collision proceeds at low velocity; thus the terms $\langle \psi_1 | \frac{\delta}{\delta t} | \psi_1 \rangle$ and $\langle \psi_2 | \frac{\delta}{\delta t} | \psi_2 \rangle$ are taken to be zero. This is equivalent to stating that the readjustment time taken by the orbitals during the collision is very short compared to the total time taken by the collision. Thus, we can write (5) and (6) as

$$\dot{a}_1 = a_2 \langle \psi_1 | \frac{\delta}{\delta t} | \psi_2 \rangle e^{\frac{-i}{\hbar} \int (E_2 - E_1) dt} \quad (7)$$

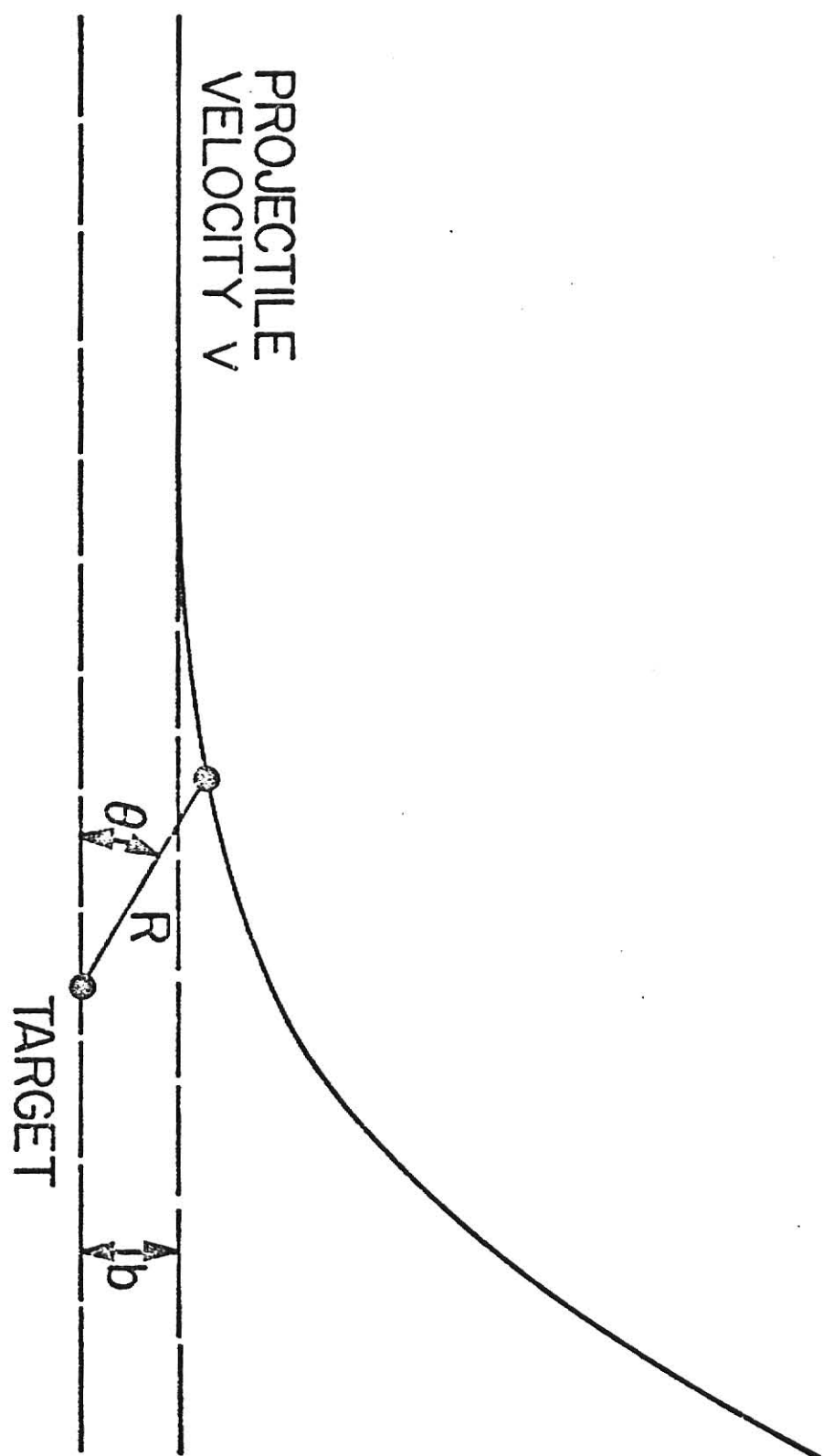
$$\dot{a}_2 = a_1 \langle \psi_2 | \frac{\delta}{\delta t} | \psi_1 \rangle e^{\frac{+i}{\hbar} \int (E_2 - E_1) dt} \quad (8)$$

Using the chain rule, the time derivative becomes

$$\frac{\delta}{\delta t} = R \frac{\delta}{\delta R} + \Theta \frac{\delta}{\delta \Theta} \quad (9)$$

The first term on the right hand side of (9) represents a coupling which takes place at large internuclear distance R , and is accordingly called radial coupling. The second term represents a coupling which occurs at small R and is called a rotational coupling.¹⁸ Θ is the angle noted in the schematic of the collision, Figure 2; and the terms radial and rotational coupling are noted in Figure 1. The radial coupling does not

Figure 2. Schematic diagram of the collision process. The dots indicate the charge centers of the two colliding atoms; the electron clouds are omitted. b represents the impact parameter in the classical definition, and R is the instantaneous distance between the charge centers. The collision occurs in the XZ plane, with the Y axis coming out of the plane and the initial velocity in the negative x direction.



occur unless the angular momentum projection quantum number changes by zero units (as a $1s\sigma$ to $2p\sigma$ transition); and the rotational coupling does not occur unless the angular momentum projection quantum number changes by one unit (as a $2p\sigma$ to $2p\pi$ transition). Thus, the two couplings occur independent of one another. The radial coupling will not be considered further here, as it has been previously investigated.^{12,13} It should be mentioned, however, that radial coupling must occur if the $2p\sigma$ -vacancy is to be transferred down to the K shell of Z_1 ; this is evident from Figure 1. Such radial coupling involves the sharing of the vacancy by the target and projectile as they move apart, and is not expected to be impact parameter dependent.

Referring to Figure 2 for the definition of the impact parameter b , conservation of angular momentum requires

$$m v b = m R^2 \dot{\theta} \quad (10)$$

so

$$\dot{\theta} = \frac{v b}{R^2} \quad (11)$$

Next, note that the term $\frac{\delta}{\delta\theta}$ actually is an angular momentum in the x-direction (see Figure 2), so we replace it by the proper operator:

$$\frac{\hbar}{i} \frac{\delta}{\delta\theta} = L_x \quad (12)$$

Thus, we finally have the two-state coupled equations for rotational coupling,

$$\dot{a}_1 = a_2 \frac{v b}{R^2} \langle \psi_1 | L_x | \psi_2 \rangle e^{\frac{-i}{\hbar} \int \Delta E dt} \quad (13)$$

$$\dot{a}_2 = a_1 \frac{v b}{R^2} \langle \psi_2 | L_x | \psi_1 \rangle e^{\frac{+i}{\hbar} \int \Delta E dt} \quad (14)$$

where we have defined the energy difference

$$\Delta E(t) = E_2 - E_1 \quad (15)$$

and used a transformation to get rid of the i in each equation.

These coupled equations can be solved, by using a computer, to obtain $a_1(t)$ and $a_2(t)$. The initial conditions, as used by Briggs and Macek,⁹ are

$$\begin{aligned} a_1(-\infty) &= 1 \\ a_2(-\infty) &= 0 \end{aligned} \quad (16)$$

and the impact-parameter dependent probability that after the collision an electron has been promoted to the $2p\pi$ level (or a vacancy transferred down to the $2p\sigma$ level) is just

$$P(\theta) = |a_2(+\infty)|^2. \quad (17)$$

$P(\theta)$ is transformed into $P(b)$ by using a suitable relation between θ and b .

The results of this calculation for a given system can also be made to scale to other similar systems, as shown by Briggs and Macek,^{9,19} and by Taulbjerg, et al.,^{11,20,21}. The fact that these results scale easily for many collision systems is quite important, for it shows that some fundamental symmetry for collisions has been found. The nature of this scaling is that the energy difference ΔE and the matrix elements in (13) and (14) behave like universal functions and scale with the atomic numbers of the projectile and target atoms. The suggestion that the energy difference and the matrix elements are universal functions is amenable to experimental testing. Taulbjerg, et al.,¹¹ have constructed tables of $P(b)$ based on this assumption of universality, which describe rotational

coupling for collisions between atoms of the first row in the periodic table rather well. The purpose for performing the experiment described in the following sections is to test whether the predicted $P(b)$ functions continue to fit the data for collisions with a higher average atomic number Z than has been previously tested, and to determine whether the two-step process described in Chapter 1 is operating for such high- Z collisions.

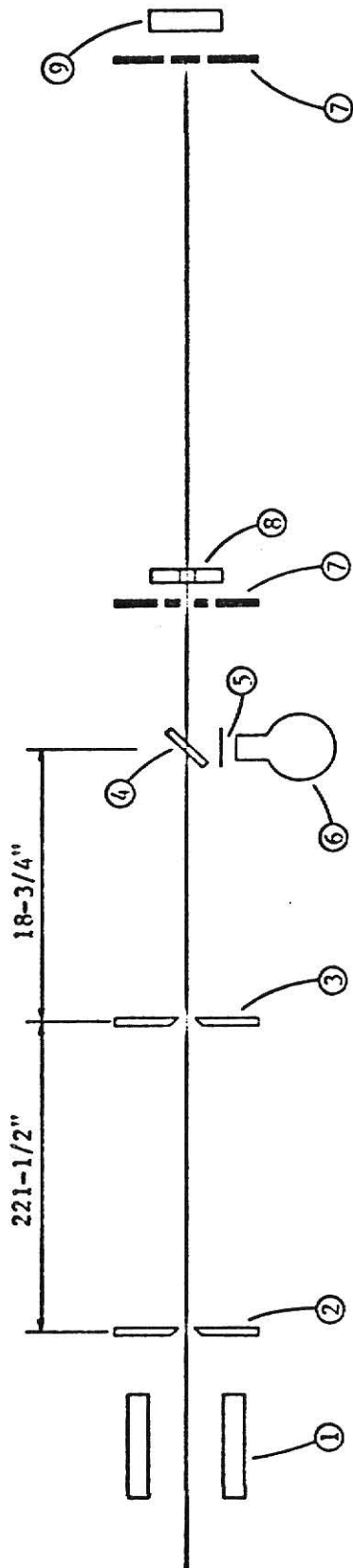
III. Experimental Method and Data

Thin solid nickel targets were prepared by evaporating powdered nickel metal onto $5 \mu\text{g}/\text{cm}^2$ ($\pm 10\%$) Arizona carbon foils in a vacuum evaporator. In constructing the thicker foils, it was necessary to use repeated evaporations to achieve the desired thickness. The target foils were floated onto aluminum target holders having a 3/16 inch hole. The extreme thinness of the foils caused a continuing problem with breakage, and many of the foils were lost in minor vacuum incidents during the course of the experiment.

Beams of Cu^+ ions were produced by a Universal Negative Ion Source (UNIS) and injected into the Kansas State University 6MV model EN Tandem Van de Graaff accelerator. The most abundant isotope was chosen, since the experiment was expected to show no isotope effects. After acceleration to 50 or 65.6 MeV (scaled velocity $v/v_e = 0.21$ or 0.27 , respectively), they were separated according to energy by a magnetic analyzer. The chosen beam was focused by a quadrupole magnet, and a pair of four-jaw slits defined its size and trajectory. A beam spot of less than 1.5 mm in cross section was maintained at all times, and in general slit scattering was not a problem. The tight beam colimation was necessary to maintain low uncertainty in the measurement of the impact parameter.

The experimental apparatus is shown in Figure 3. Target foils were mounted on a fixture which allowed any of five targets to be placed in front of the beam without opening the evacuated chamber, and which allowed a full 360° rotation of the chosen target. The effective thickness of the target could be changed by changing the target's angle with respect to the beam.

Figure 3. Diagram of the experimental apparatus. The copper beam enters from the left, after magnetic energy sorting has taken place.



- | | |
|-----------------------|-----------------------------------------------------------------|
| ① QUADRUPOLE MAGNET | ⑥ S4(L4) DETECTOR |
| ② 4-JAW SLITS | ⑦ ANNULUS |
| ③ 4-JAW SLITS | ⑧ ANNULAR SURFACE BARRIER DETECTOR
FOR RUTHERFORD SCATTERING |
| ④ TARGET | ⑨ DOWNSTREAM SURFACE BARRIER
DETECTOR |
| ⑤ POLYETHYLENE WINDOW | |

Nickel $K\alpha$ X rays (8.3 keV) from the target were detected in coincidence with the scattered copper particles from the beam. The simultaneous detection of an X ray and a scattered particle signaled that a K-ionizing event had taken place. The electronics required for this measurement are shown in Figure 4. All the electronics units are standard NIM modules except the multi-channel analyzer and the PDP-15 computer.

In the initial experiments, X rays were detected with an Ortec Si(Li) detector. Later in the experiment, the Ortec detector was replaced by a Kevex Si(Li) detector having somewhat better energy resolution and greater solid-angle efficiency (approximately one percent overall). A 7.5 mil (nominal) polyethylene absorber was placed over the Si(Li) detector window to reduce the background of copper and nickel L X rays. This absorber was found to have a transmission of .89 for the nickel $K\alpha$ X rays.

The scattered copper particles were collected downstream by a surface barrier detector. This detector was mounted on a micrometer head so that it could be scanned in the x and y directions perpendicular to the beam, and thus the beam center could be easily located. A stainless-steel annulus was placed over the detector to select the viewing angle. Because of the low coincidence count rate for the experiment, it was found necessary to use the annulus and count in a nearly- 2π geometry rather than simply count with a pinhole over the detector. A set of annuli with mean diameters ranging from 7 mm to 18 mm was used. The scattering angle θ was determined by the radius of the annulus and by the distance from the target to the surface-barrier detector, which was varied from 8.75 inches to 34 inches by changing the beam pipe itself. This combination of annuli and beam pipes allowed measurements to be made for impact parameters of approximately 300 to 4000 Fermi (.003 to .04 Angstrom).

Figure 4 Block diagram of the coincidence electronics used for the impact-parameter measurements. All units are standard NIM modules.

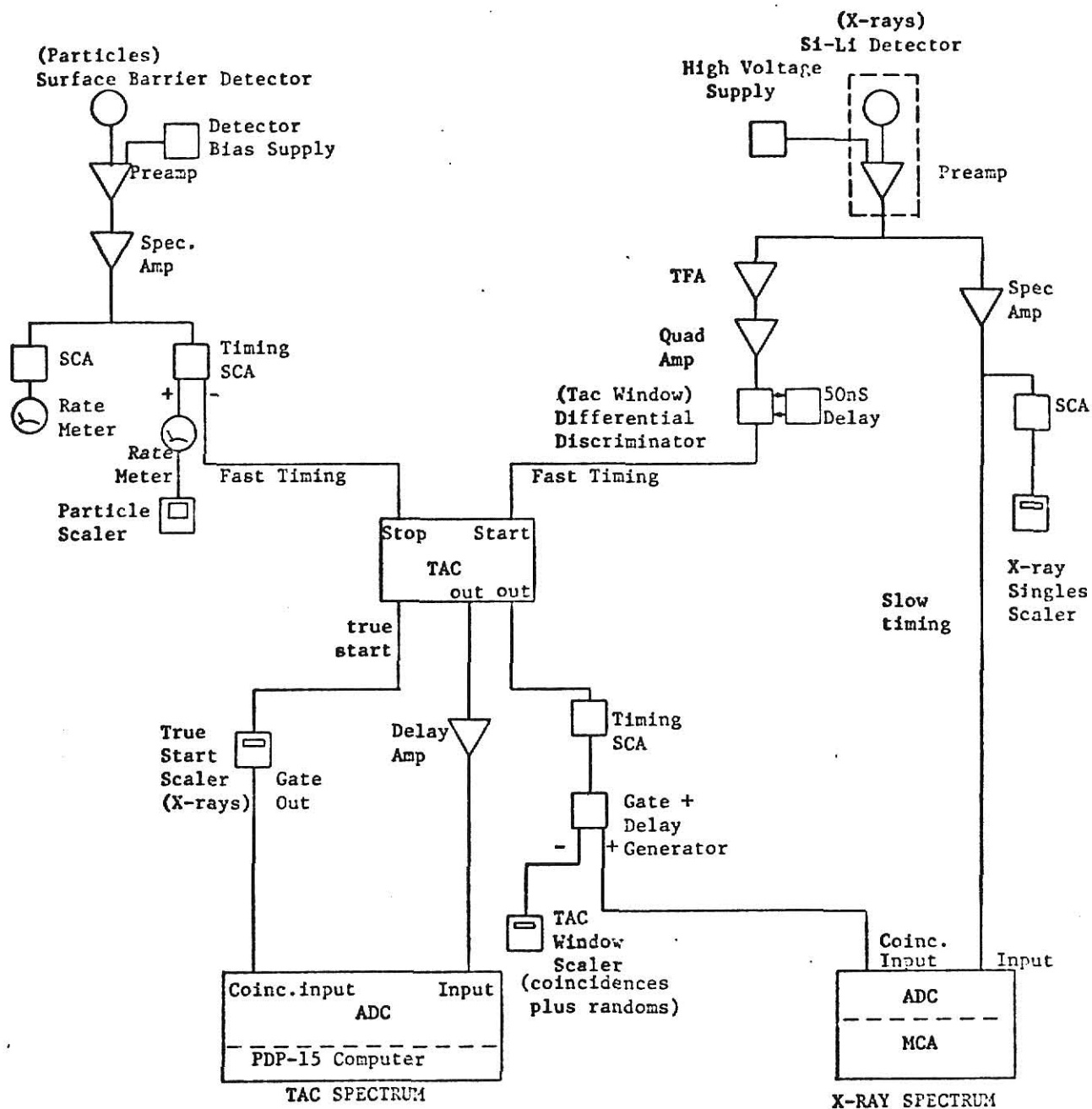
Abbreviations: ADC - analog-to-digital converter


 MCA - multi-channel analyzer

 SCA - single-channel analyzer

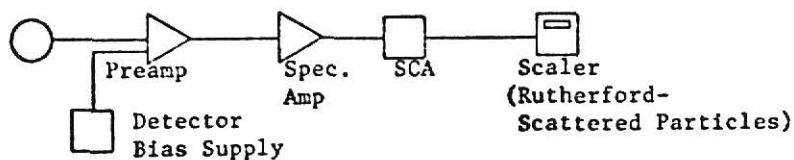
 TAC - time-to-amplitude converter

 TFA - timing filter amplifier



 Time Scaler
(Master for all scalers)

(Rutherford Monitor)
Surface Barrier Detector



For the purpose of designing the experiment, the impact parameter b may be estimated by using the Rutherford formula,

$$b = \frac{Z_1 Z_2 e^2}{E \theta} \quad (1)$$

where

Z_1 = atomic number of the target atom (28 for nickel)

Z_2 = atomic number of the projectile atom (29 for copper)

e^2 = 1.44 MeV-Fermi

E = projectile energy in MeV

θ = scattering angle in radians.

However, since the scattering potential is more complex than the simple Coulomb potential used in Rutherford scattering, a better relation between impact parameter and measured scattering angle is needed for final analysis of the data. Using the method of Everhart, Stone, and Carbone,²³ a screened-Coulomb impact parameter may be obtained for each scattering angle. An explanation of this method, along with the computer code used in the calculation, is contained in Appendix A. Results of the calculation are shown in Figure 5. All succeeding figures are plotted with screened-Coulomb impact parameters.

The TAC spectra obtained in coincidence runs were digitized and stored by the PDP-15 computer. A typical TAC spectrum for a 50 MeV run is shown in Figure 6. Coincidence x-ray spectra were stored in a Canberra multi-channel analyzer (MCA). A typical x-ray spectrum for a 50 MeV coincidence run is shown in Figure 7. All spectra were transferred to magnetic tape after every four runs, thereby preserving them for further examination at a later date.

Figure 5. Results of the calculation of Appendix A which relates the measured angle of the scattered particle and the screened-Coulomb impact parameter for copper on nickel. The range of data covered by this experiment is also indicated. The curve marked R denotes the Rutherford impact parameter; the line marked SC denotes the screened-Coulomb impact parameter.

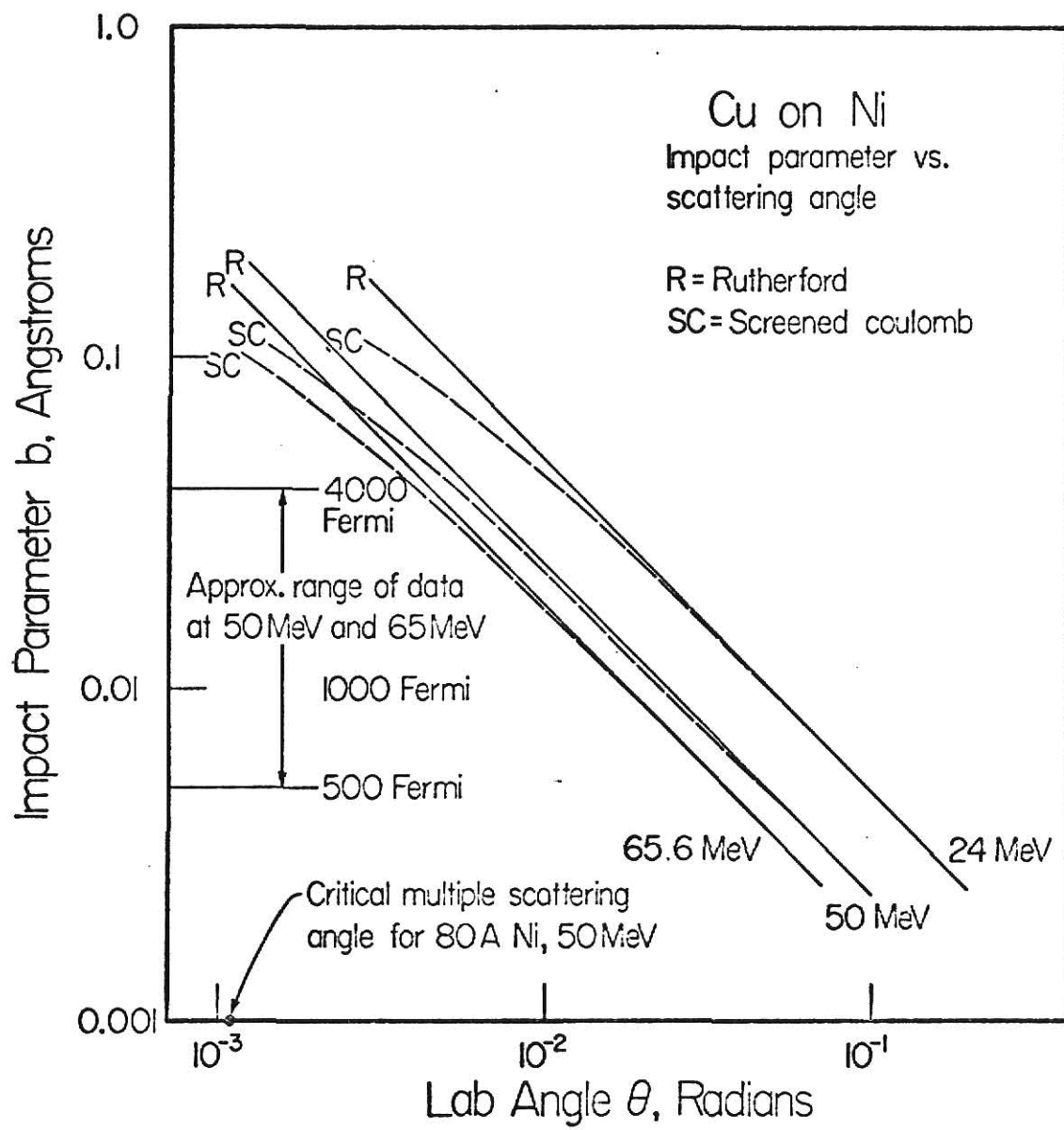


Figure 6. Typical coincidence TAC spectrum obtained for 50 MeV run.
The spectrum is taken for an impact parameter of $b = 2368$
Fermis and 3.91 Nanoseconds/channel.

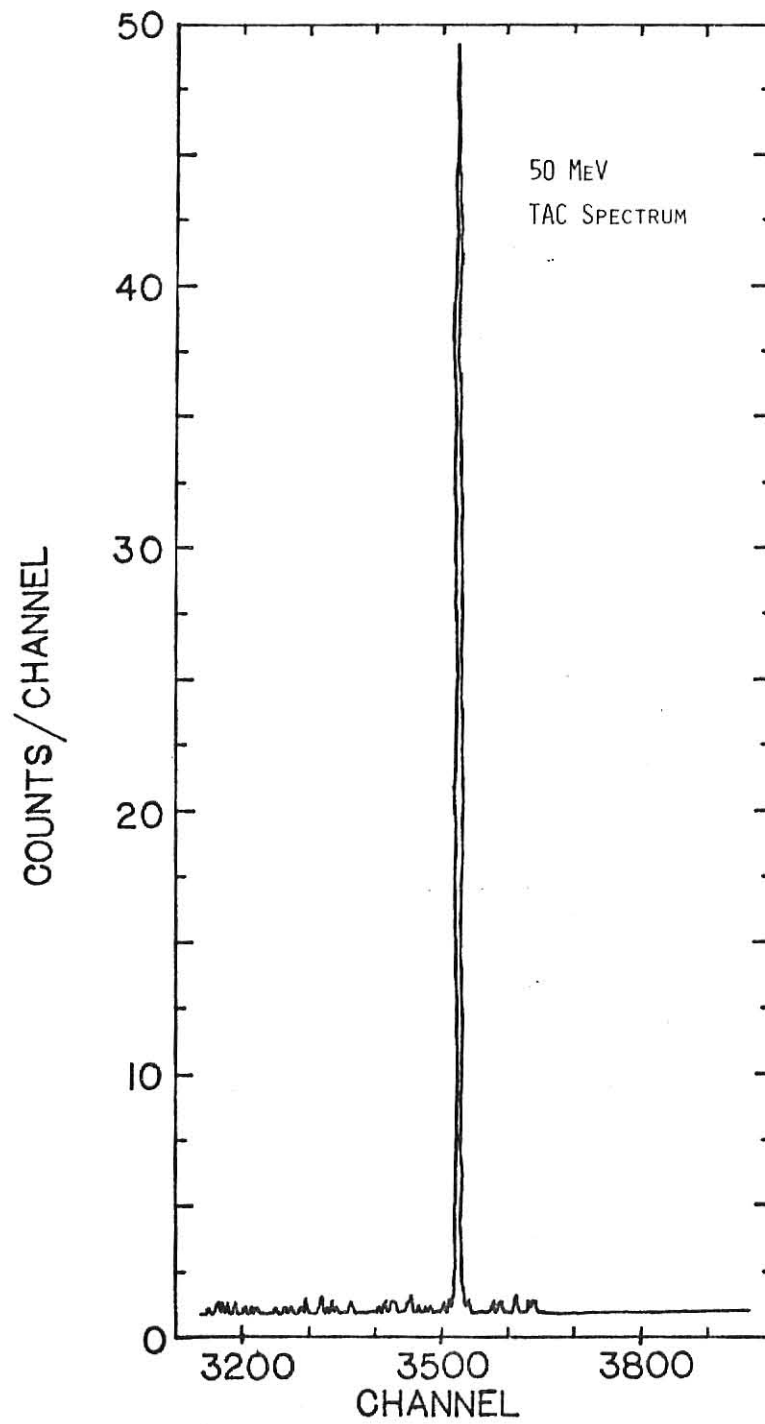
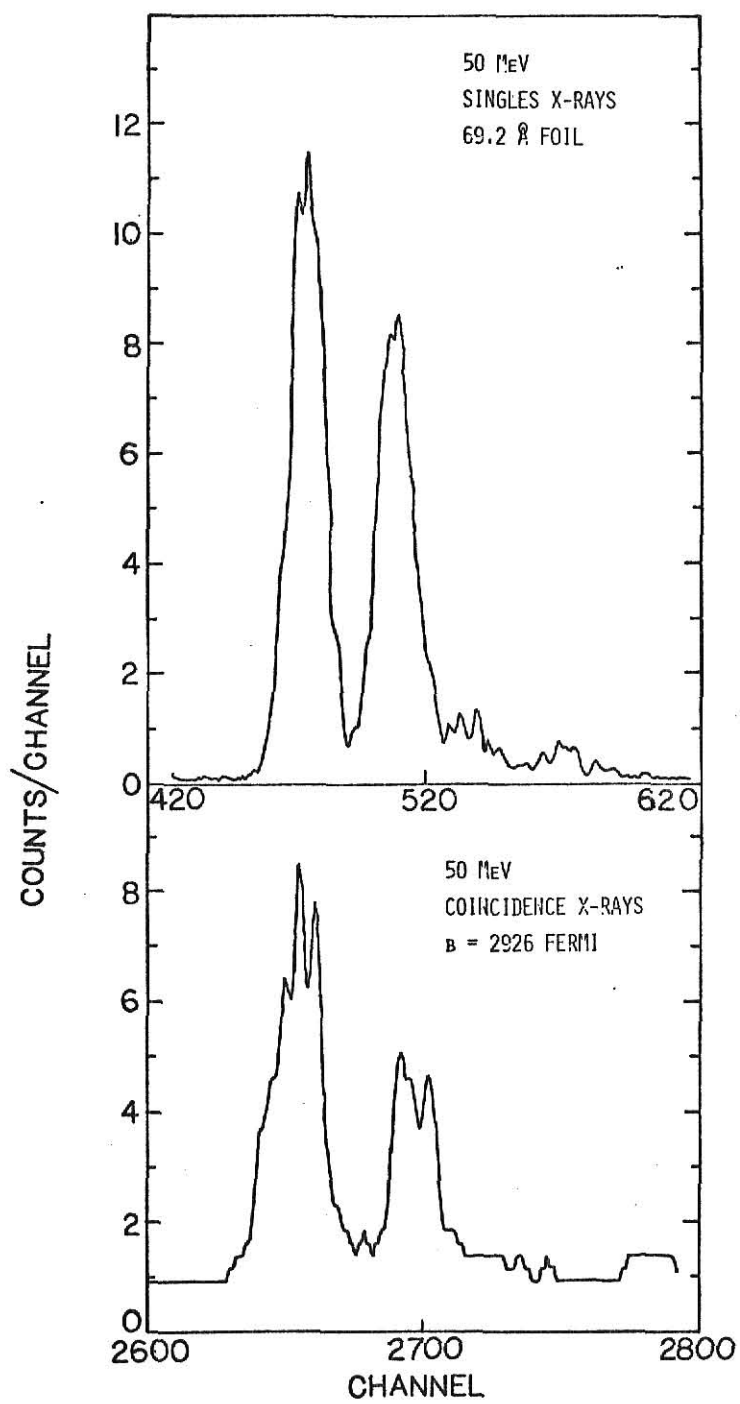


Figure 7. Typical x-ray spectra obtained for 50 MeV runs. The upper spectrum is the singles X rays for a 69.2 \AA nickel foil, obtained with no coincidence requirement; the lower spectrum is a coincidence data run for an impact parameter of 2926 Fermi. The large peak at the left is the nickel $K\alpha$ X ray; the right peak is the copper $K\alpha$ X ray. Actual channel numbers are shown; the zeroth channel has been suppressed.



The true thickness of the nickel on the foils was determined by two methods. In the first, protons of several keV were produced in the 3 MV model AK-N Van de Graaff Accelerator ("Baby Huey") and scattered off the foils in 20-second timed runs. The scattering from nickel was compared to that from a commercially-prepared electro-deposited 1524 Å nickel foil with no carbon backing, and the true foil thickness is then

$$\text{true foil thickness} = 1524 \text{ Å} \frac{(\text{\#protons scattered from foil})}{(\text{\#protons scattered from 1524 Å foil})} \quad (2)$$

It was later found that the same results could be obtained by examining the singles Rutherford scattering from the foil in timed runs when it was bombarded by the copper beam at 50 or 65.6 MeV. Again, the 1524 Å foil was used as the standard.

During an attempt to extend the data to 25 MeV, it was discovered that the copper ion beam has an extremely destructive effect on the targets and on the surface barrier detector. The 25 MeV runs were abandoned because the target foil thickness changed as much as 50% during the course of a run at a single impact parameter, making the data impossible to interpret. Following this experience, a particle detector was installed at a large angle (about 12 degrees) to monitor beam particles Rutherford scattered from the target foil and thus give some indication as to whether the foil thickness was changing. In its final form, this monitor was an annular surface barrier detector with an annulus to select the viewing angle, as indicated in Figure 3. At 50 to 65.6 MeV, the target thickness change is essentially zero.

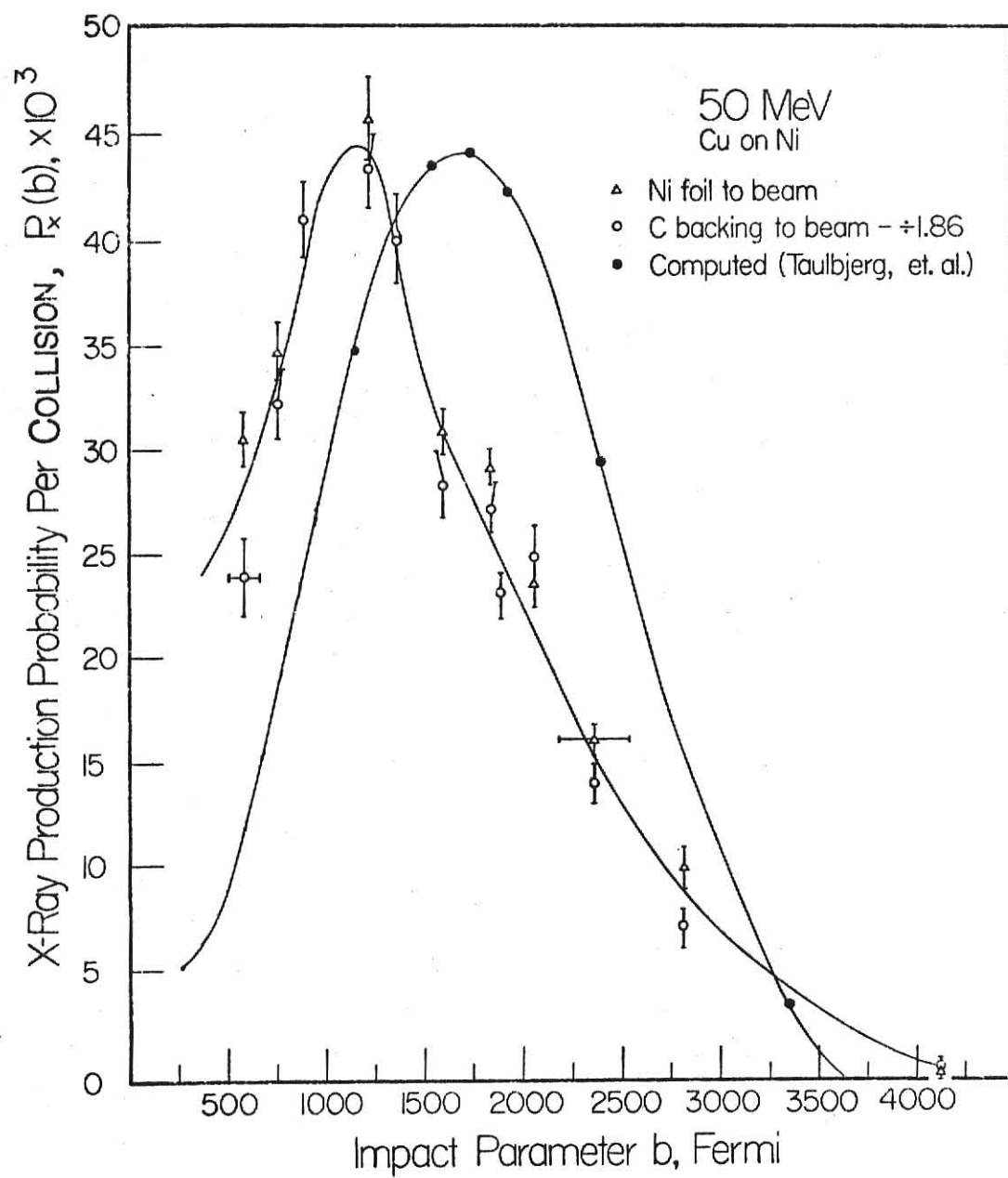
From Figure 1, it is evident that $2p\pi$ vacancies are necessary for the expected rotational coupling process to occur. Conversely, if $2p\pi$ vacancies are known to be present, rotational coupling is expected. The $2p\pi$

vacancies can be brought into the collision if the charge state of the accelerated copper beam is high. The charge state of the copper beam was kept low--usually $9+$ or $10+$. With no $2p\pi$ vacancies brought in, the vacancies necessary for rotational coupling will have to be produced by another method.

The experiment measures $P_x(b)$, the nickel K x-ray production probability per collision as a function of impact parameter b . This probability is directly proportional to the vacancy production probability for the K-electron. The initial data were taken at 50 MeV; it was desired to take the second data set at 75 MeV, but the limitations imposed by the 6 MV terminal voltage of the accelerator allowed only 65.6 MeV.

The 50 MeV data is shown in Figure 8. $P(b)$ was measured for each b with the foil in two orientations: Nickel side to the beam, and turned 180° so the beam passed through the carbon backing first. The carbon backing created L vacancies in the copper beam, which became the necessary $2p\pi$ vacancies to produce rotational coupling (See Figure 1). The curves obtained for the two orientations of the foil have the same shape and exhibit the characteristic falling-off of $P(b)$ for impact parameters much less than the K-shell radius (which is 1921 Fermis for nickel). Furthermore, the carbon-first curve lies a factor of 1.86 higher than the nickel-first curve. This is consistent with the result expected from the two-step (rotational coupling) process explained in Section 1. That is, the magnitude of $P(b)$ should scale up or down only with the number of $2p\pi$ vacancies brought into the collision, and the carbon-first data is expected to lie higher because the carbon backing creates the extra L vacancies prior to the collision. The two curves would not be expected to be so simply related if a direct, one-step ionization process (see Chapter 1) was operational. It remains to be investigated

Figure 8. Nickel K_{α} x-ray production probability per collision $P_x(b)$ versus impact parameter b , data for 50 MeV. The computed curve is from Taulbjerg, et al., reference 11. The correction for finite angular resolution, described in Section IV, has been included.



whether the L-vacancies necessary for the apparent rotational coupling in the nickel-first data are created in multiple collisions prior to the collision of interest or are created in the collision of interest itself. The foil used for the data of Figure 8 had 72 Å of nickel deposited on a 5µg/cm² carbon backing.

The theoretical prediction of Taulbjerg, et al.,¹¹ for P(b) is also plotted in Figure 8. Most notable is the discrepancy between the impact parameters of the peaks in the two curves, which was very unexpected. A re-examination of an earlier experiment²⁵ shows that a small discrepancy was noted in near-symmetric chlorine-argon collisions at 15 and 30 MeV, but it was apparently not considered significant at the time.

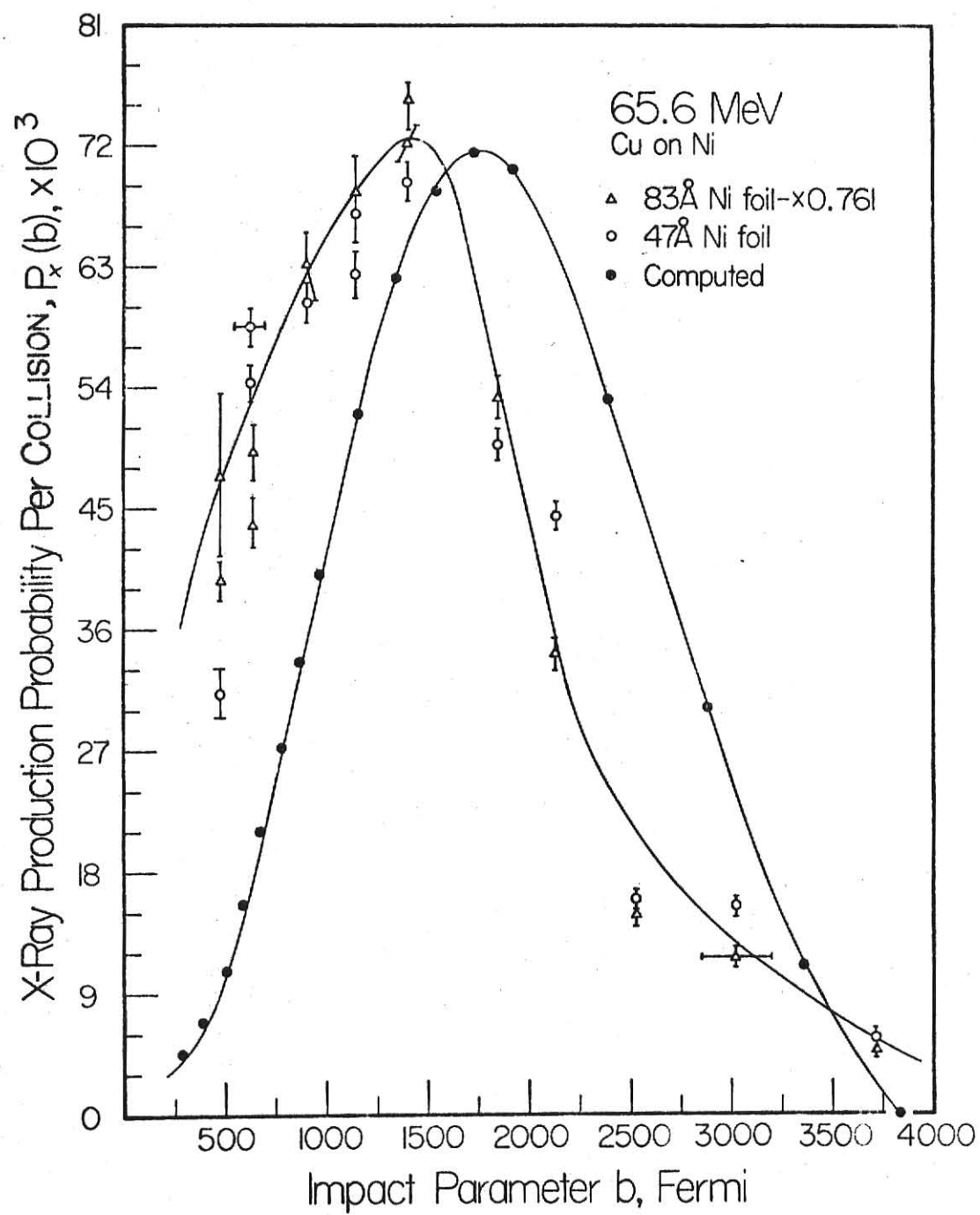
Figure 9 shows the 65.6 MeV data. This data was taken on foils of nickel thickness 47 Å and 83 Å. Again, when the data for the 83 Å foil is multiplied by 0.761, it lies on the same curve as the data for the 47 Å foil. The prediction of Taulbjerg, et al.,¹¹ is also shown, and again a discrepancy exists in the position of the peak. It should be noted that for both sets of data, the theoretical predictions were normalized to match the experimental peak heights in order to facilitate comparison of the two curve shapes. To convert the measured P_x(b) to a 2pσ vacancy production probability P_{2pσ}(b), the formula to use is

$$P_{2p\sigma}(b) = \frac{P_x(b)}{f_{Ni} \omega_K} \quad (3)$$

where ω_K is the K-shell fluorescence yield for nickel and f_{Ni} is the fraction of nickel K_α X rays/total copper plus nickel K X rays observed in coincidence runs. This equation is derived in Appendix C.

The discrepancy between theory and experiment constitutes a significant result, as tests of the theory for collisions of such a high average Z have not appeared in the literature (but the theory is known to work very well for collisions of lower Z).

Figure 9. Nickel K_{α} x-ray production probability per collision $P(b)$ versus impact parameter b , data for 65.6 MeV. Data is given for two foil thicknesses, with the thicker foil normalized to the thinner. Again, the computed curve is from Taulbjerg, et al., reference 11, and the correction of Section IV for finite angular resolution has been included.



IV. Solid Target Effects and Corrections to Data

In any experiment using a solid target of nonzero thickness, multiple scattering of the projectile atom from the atoms in the target is inevitable. However, for the purposes of this experiment a distinction may be made between the effects of multiple scattering which are desirable and those which are detrimental to the interpretation of the data. The desirable effect of multiple scattering occurs prior to the collision which produces a K-vacancy; the projectile scatters off the target atoms in such a way that its trajectory does not necessarily change, but L-shell vacancies are produced in it. In this way, the $2p\pi$ vacancies necessary for rotational coupling are available when the projectile finally interacts with a target atom and produces K-vacancies. On the other hand, the multiple scattering (before or after the vacancy-producing collision) may occur in such a way that the projectile is re-scattered, so that the impact parameter at which it is detected is not the impact parameter which results from its vacancy-producing interaction with a target atom. Hence, the measured $P(b)$ may be in error by various amounts according to the value of impact parameter b . This detrimental effect of multiple scattering appears in the apparatus as finite angular resolution, and a correction to the data is necessary. Because of the very small angles at which the data is taken, the correction for finite angular resolution has the potential for being quite large. This chapter will examine the effects of multiple scattering, both desirable and detrimental, on the data.

First, consider the detrimental effect of finite angular resolution. As a beginning, an estimate for the critical angle at which multiple scattering becomes important may be made.²⁸ The critical angle is given by

$$\theta_{\text{CRITICAL}} = \left[\frac{n \pi t Z_1^2 Z_2^2 (e^2)^2}{E^2} \right]^{1/2} \quad (1)$$

where θ_{CRITICAL} is in radians,

n is the number density of atoms in the target,

Z_1 is the atomic number of the projectile atom,

Z_2 is the atomic number of the target atom,

e^2 is given the value 1.44 MeV-Fermi,

t is the thickness of the target foil,

E is the energy of the projectile in MeV.

This calculation gives the values

$$\theta_{\text{CRITICAL}} = 1.12 \times 10^{-3} \text{ radian for } 83 \text{ } ^0\text{Ni at 50 MeV}$$

$$\theta_{\text{CRITICAL}} = 4.45 \times 10^{-4} \text{ radian for } 5 \mu\text{g/cm}^2 \text{ carbon at 50 MeV.}$$

The angular range of the data is indicated on Figure 5. Clearly, multiple scattering from the carbon backing will not be a problem; however, the approximate nature of the equation dictates a large error bar on the nickel result, and, thus, the correction of undesirable multiple scattering from nickel must be attended to more carefully. Similar results may be found for the 65.6 MeV data.

To obtain a further idea of the extent of undesirable multiple scattering effects and finite angular resolution, a baffle with a 1 mm hole was placed over the downstream surface barrier detector and the beam profile was obtained. As is evident from Figure 10, insertion of the

target foil causes some spreading of the beam profile, indicating that undesirable multiple scattering is taking place. However, again the magnitude of the undesirable effect is not great.

All the undesirable effects of finite angular resolution can be removed from the $P_x(b)$ data. Using a method similar to that used by R. Randall,²⁶ the data is replotted using the weighted average angle $\langle\theta\rangle$ instead of the measured angle θ to determine the impact parameter. A program written by Dr. C. L. Cocke for the HP-67 pocket calculator was used to generate the universal curve of Figure 11, which relates the weighted average angle to the measured angle. The universal curve is in units of σ , the half-width of the beam profile (Figure 10) where it drops to $1/e$ of its peak value. This correction has been applied to the data presented in Figures 8 and 9, so that the effects of finite angular resolution are removed.

Now, consider the magnitude of the desirable effect. In order to get an idea of the behavior of the beam inside the foil, a carbon post-stripping foil was inserted into the beam between the accelerator analyzing magnet and the beam-line switching magnet. In this way, the switching magnet could be used to sort the beam by charge state. A carbon foil was used because of the 50 MeV carbon-first data, which argues strongly that L-vacancies are produced in the beam prior to its entering the nickel. For 50 MeV, the fraction of each charge state emerging from the foil is shown in Figure 12. The equilibrium charge state distribution of the emerging copper beam shows substantial fractions of L-vacancy-bearing Copper ions. When compared with the charge state of 9^+ that goes into the foil, this gives some idea of the effectiveness of multiple scattering in producing vacancies in the beam.

With the coincidence requirement removed, the total nickel K x-ray yield was measured as a function of target thickness at 50 MeV. This data is shown in Figure 13. The growth of the x-ray yield can be interpreted as due to the growth with target thickness of the number of 2P vacancies in the projectile. The curve shows that equilibration between the production and destruction of 2P vacancies in the copper beam occurs at a target thickness of about 100 \AA . In addition, the plot of nickel K x-ray production probability $P(b)$ as a function of target thickness for several impact parameters, Figure 13, shows that the magnitude of the $P(b)$ curves scales with the apparent measured total x-ray production cross section.

The fact that the total x-ray production cross section (x-ray yield) is nonzero when extrapolated to zero target thickness (see Figure 13) is important and can be interpreted along previously published lines.²⁵ At zero target thickness, pure single-collision conditions exist. The fact that the K x-ray yield does not drop to zero at zero target thickness indicates that the rotational coupling process is still operative even though no copper L vacancies are being brought in by the copper projectile atoms. An explanation for this apparent paradox is that now the molecular orbitals higher than $2p\pi$ are participating somehow. In a single collision, vacancies are being produced in the orbitals which the model of Section I has neglected, and these vacancies are working their way down to the $2p\pi$ orbital so that rotational coupling can occur at zero target thickness. Another way to state this is to say that the basis set for the calculation of Section II would have to be expanded. Normally, these higher orbits are neglected because their effects occur only at much larger impact parameters than these experiments look at; however, here they seem to be

27

28

29

30

31

Figure 10. Plot of count rate versus distance from beam center for scans through the copper beam at 50 MeV. The difference in the half widths at $1/e$ of maximum is not great, indicating that unwanted multiple scattering is not a problem for the $P(b)$ data.

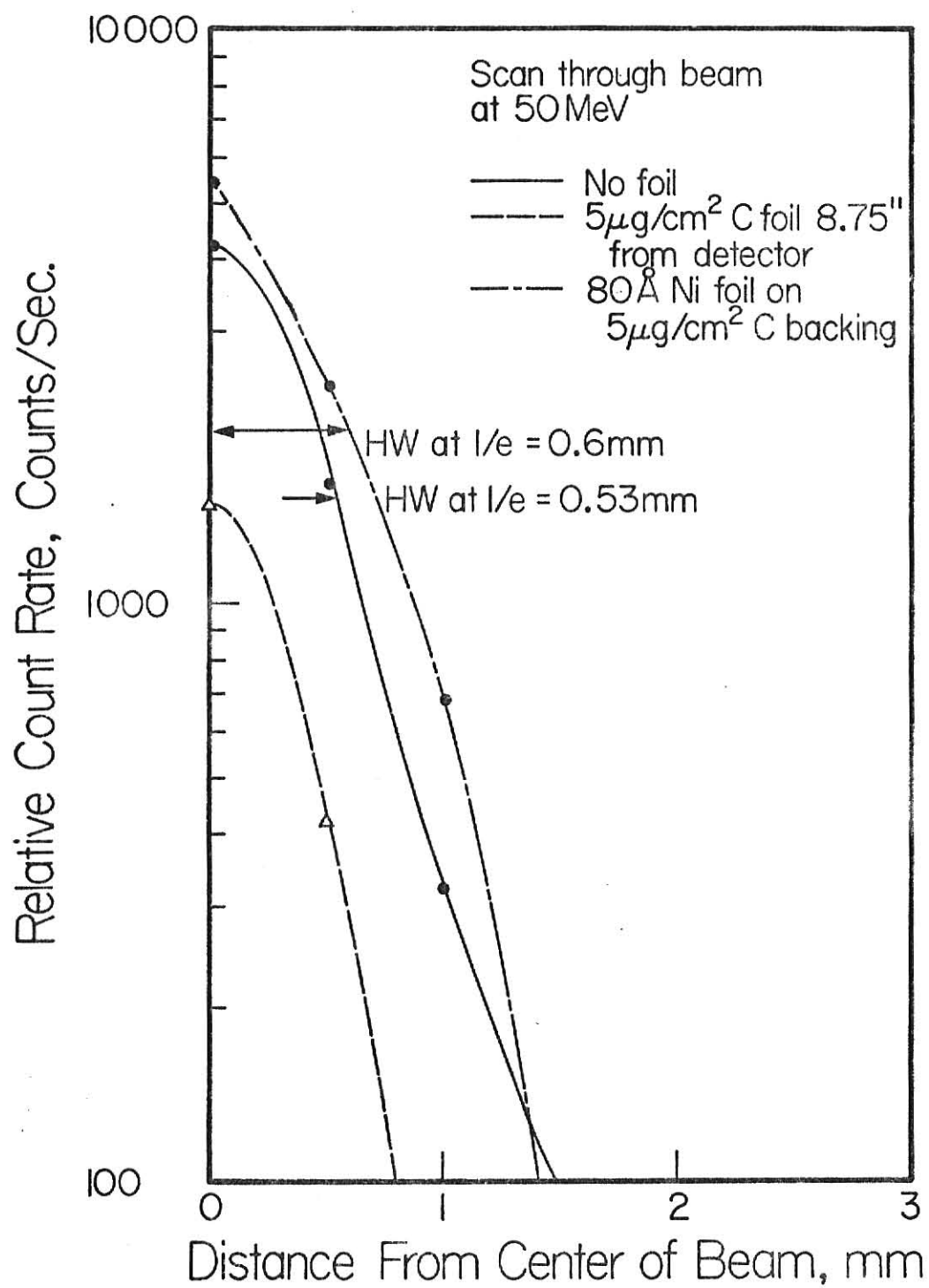


Figure 11. Universal curve used to correct the $P(b)$ versus b data for finite angular resolution at small angles. θ is the measured angle at which data was taken, $\langle\theta\rangle$ is the weighted average angle assuming Rutherford scattering, and σ is the angle of the half-width at $1/e$ taken from the beam profile curve (Figure 12). This curve is used in conjunction with Figure 5 when correcting the $P(b)$ data.

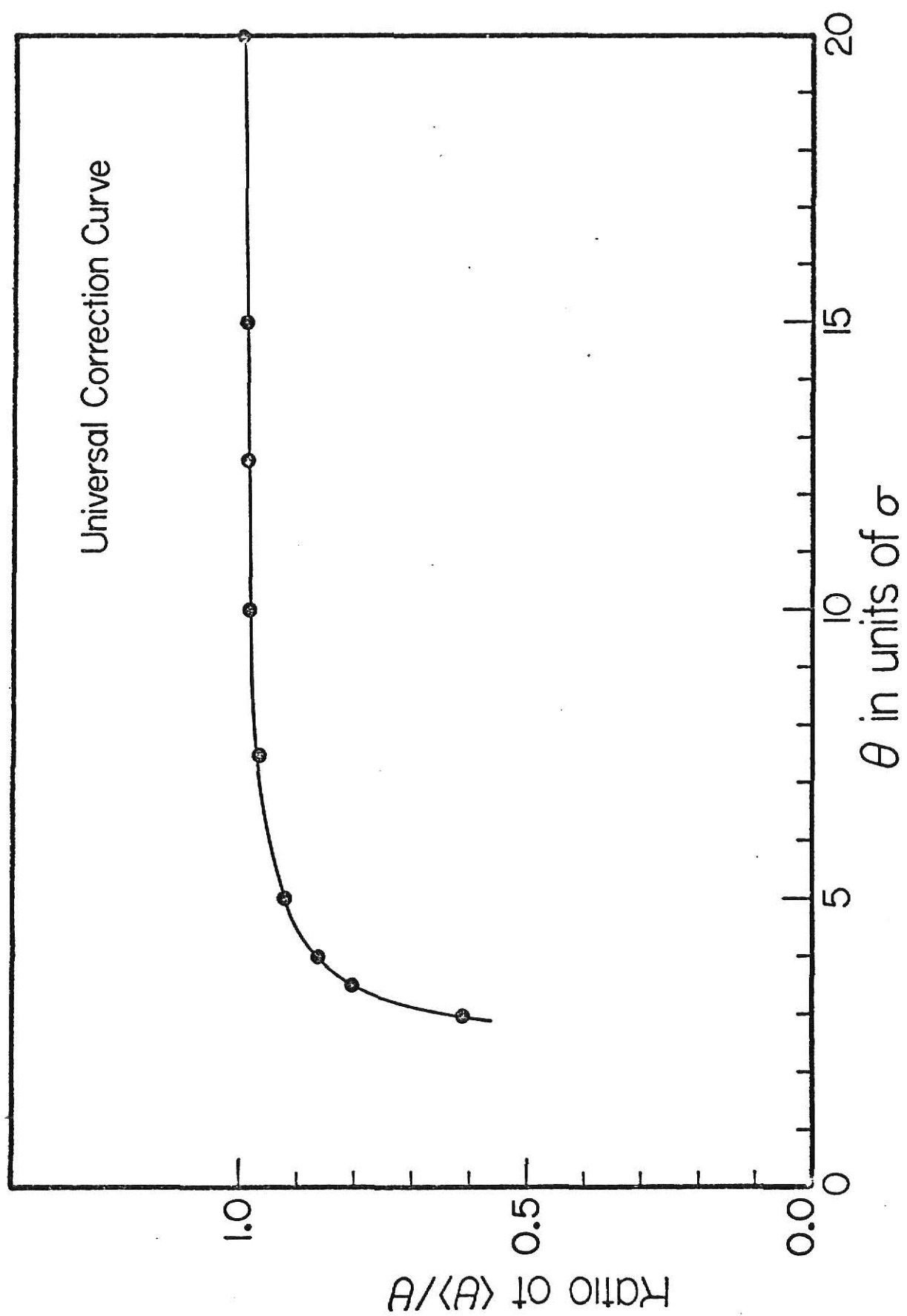


Figure 12. Histogram showing the relative amount of each charge state of the copper beam emerging from a $5\mu\text{g}/\text{cm}^2$ carbon foil at 50 MeV.

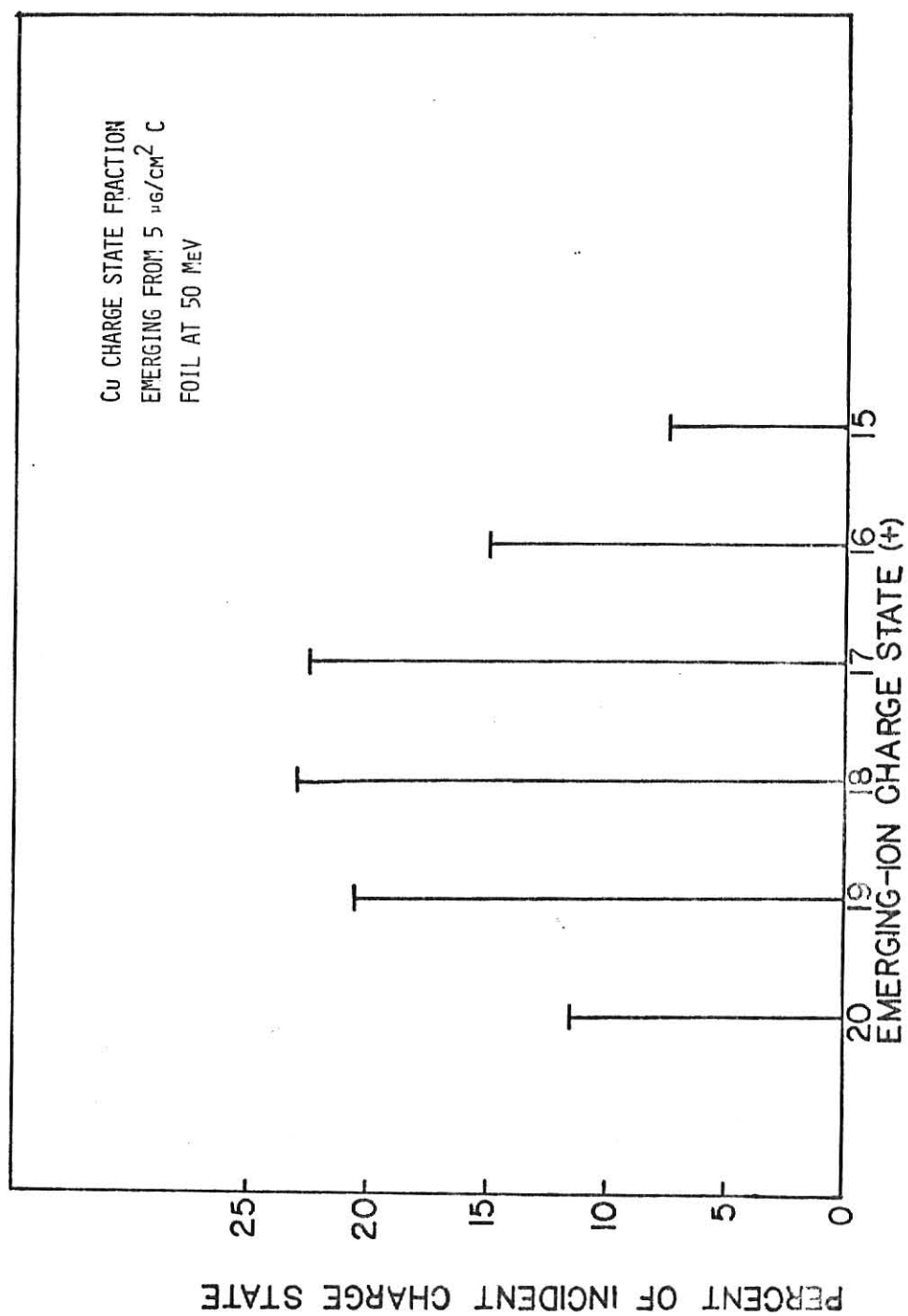
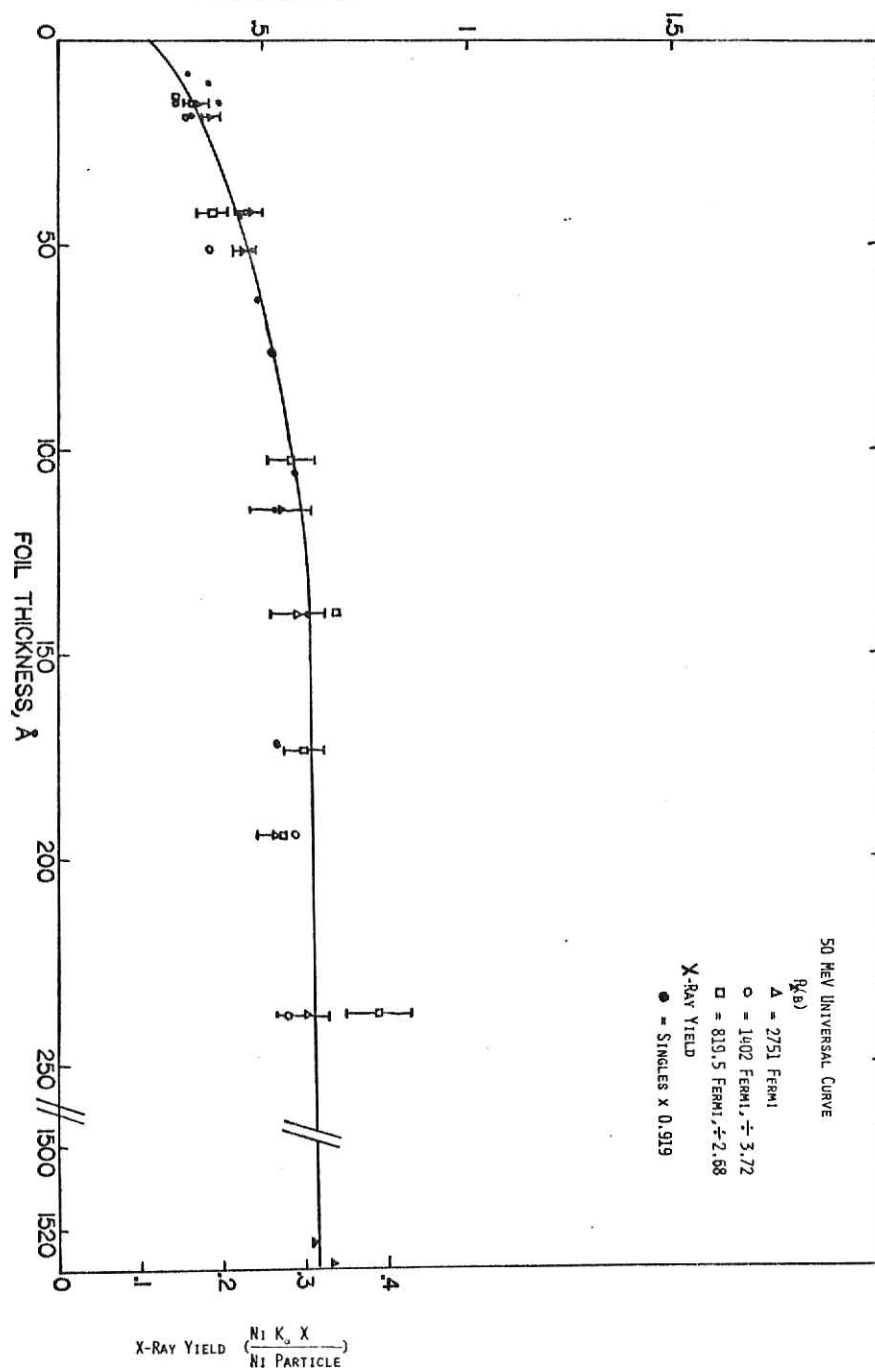


Figure 13. Data of total x-ray yield versus nickel foil thickness and nickel K x-ray production probability $P_x(b)$ versus nickel foil thickness at 50 MeV. The $P_x(b)$ data for three impact parameters and the x-ray yield data have all been normalized to lie on the same universal curve. The data may be fit by the curve $P_x(b) = .004 (1 - e^{-\frac{t}{60}}) + .0023$ where t is the foil thickness in Angstroms.

NICKEL K_{α} X-RAY PRODUCTION PROBABILITY PER
PARTICLE, $P_X(b) \times 10^{-2}$



involved with the process. In this experiment it is not possible to ascertain the nature or mechanism for vacancy production in the higher molecular orbitals and their subsequent transfer downward.

It is important to know whether the targets used for these measurements were uniformly evaporated or whether clumping of the nickel occurs. If the nickel is clumped or non-uniform, the thickness of the target may not be what the number density measurement indicates (especially for targets this thin), and the x-ray yield versus thickness curve in Figure 13 may not be correct (causing the interpretation above to be incorrect). One of the targets used in the experiment was mounted on a fine copper grid and examined in an Hitachi HU-11B transmission electron microscope. No clumping of the nickel was observed for regions as small as 200 \AA across, and a turned up edge of the foil (an artifact of transferring the foil from the target holder to the electron microscope copper grid) clearly showed that foils as thin as 80 \AA are continuous.

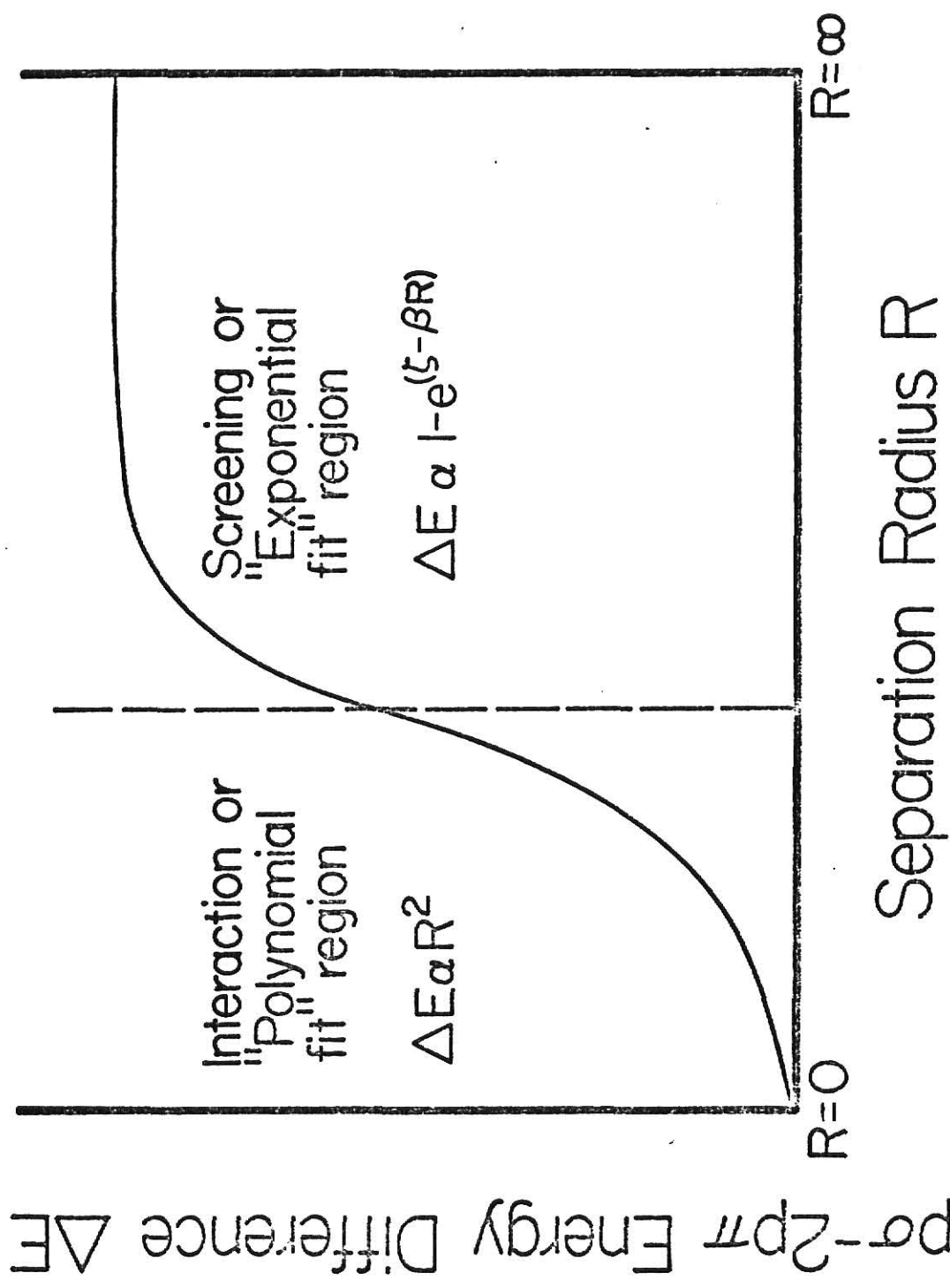
V. Revisions to Theory and Conclusion

As noted previously, careful checks on the data and evidence for the same effect in other experiments provide confidence that the discrepancy between theory and experiment is real. It is therefore necessary to attempt to reconcile the difference in some manner. Two possible explanations can be considered.

It might be argued that rotational coupling is not taking place at all, and thus the probabilities calculated by Taulbjerg, et al.,¹¹ are not applicable to this situation. However, this argument can largely be discounted on the basis of evidence presented in Sections III and IV. The qualitative shape of the observed $P_x(b)$ curve and the scaling of its magnitude with the number of vacancies brought into the collision both tend to support the presence of a rotational coupling mechanism. A calculation of $P(b)$ for the direct process described in Section I has not appeared in the literature, but such a calculation is not believed likely to show a falling-off for impact parameters less than the K-shell radius.

In explaining the molecular orbital model in Section I, the exact form of the correlation diagram was not considered important. However, in the detailed calculation of atomic collision properties, the results are found to be very sensitive to the specific form and details of the correlation diagram. In the particular case of $2p\sigma$ - $2p\pi$ rotational coupling, the energy difference ΔE between the $2p\sigma$ and $2p\pi$ molecular orbital levels is the important factor. Figure 14 shows the qualitative features of this energy difference as a function of the radius of separation R . At very small separations, the energy difference is given by a polynomial. Taulbjerg, et al.,¹¹ fit this section by

Figure 14. Detail of the two regions of the $2p\sigma$ - $2p\pi$ energy difference ΔE used in computing the $P(b)$ versus b curves for rotational coupling. The separation radius R is the distance between the two nuclei at various times during the collision.



$$\Delta E = \frac{1}{40} R^2 C \quad (1)$$

where C is the factor used to scale the energy difference properly for the system in question. The factor 1/40 is computed on the basis of a well-known formula²⁷ derived in an earlier work.

At large radius R, the energy difference changes and may be fitted by an exponential of the form

$$\Delta E \propto 1 - e^{(\gamma - \beta R)} \quad (2)$$

where γ is a constant. The region of large separation represents the portion of the collision where screening effects are important.

A computer code written by C. L. Cocke and described in Appendix B was used to investigate the effect of changing the energy difference upon the b position of the peak P(b). Although not as accurate or sophisticated as the methods used by Taubjerg to compute the P(b) (reference 11), the program is useful to assist in the qualitative understanding of what is taking place during the collision. The program was initially set up to reproduce Taubjerg's calculations, and then the polynomial energy difference of Eq. (1) was modified by changing the numerical factor. The P(b) thus obtained is surprisingly independent of the numerical factor used, not varying by more than one part in 1000 for numerical factors of .001 to .1. However, a simple modification of the exponential energy difference's numerical factor, from Eq. (2), moves the peak in the calculated P(b) over to match the peak in the data. This is interpreted as meaning that the screening occurring at large R has a tremendous effect on the interaction at small R. The exact form of the exponential ΔE is

$$\Delta E = .375(1 - \exp(-\frac{\alpha - RZ}{1.4} s)) \quad (3)$$

where $Z_s = (Z_1 Z_2)^{1/2}$. The calculations of Taulbjerg, et al.,¹¹ are reproduced by $\alpha=0.6$; the data of Figures 8 and 9 are fit by $\alpha=0.2$ for 50 MeV and $\alpha=0.3$ for 65.6 MeV.

It would appear, then, that the universal impact-parameter dependent probabilities computed and published by Taulbjerg, et al., are not truly universal and do not scale to fit all collision systems. On the basis of the chlorine-argon data of reference 25 and the data reported herein, the discrepancy between theory and experiment appears to become worse as the average atomic number of the colliding partners increases. It would be interesting to perform further measurements of this type on systems having a higher average atomic number and see if the discrepancy continues to increase.

References

1. J. Chadwick, Phil. Mag. 24 (1912), 594; J. Chadwick, Phil. Mag. 25 (1913), 193; A. S. Russell and J. Chadwick, Phil. Mag. 27 (1914), 112; J. J. Thompson, Phil Mag. 28 (1914), 620; E. Rutherford and H. Richardson, Phil. Mag. 25 (1914), 722.
2. W. M. Coates, Phys. Rev. 46 (1934), 542; M. Tanaka and I. Nonaka, Proc. Phys. Math. Soc. Japan 20 (1938), 33.
3. E. Merzbacher and H. W. Lewis, in Encyclopedia of Physics, ed. S. Flügge, Vol. 34 (Springer-Verlag, Berlin, 1958), 166-192.
4. The corrections are detailed in reviews by J. M. Hansteen, Advances in Atomic and Molecular Physics, Vol 11 (1975), 299-329; D. H. Madison and E. Merzbacher, "Theory of Charged-Particle Excitation" in Atomic Inner-Shell Processes, ed. by B. Crasemann, (Academic Press, 1975) 2-73. See also H. O. Lutz, Proc. Second International Conf. on Inner Shell Ionization Phenomena, (ed. W. Mehlhorn and R. Brenn, Universität Freiburg, FRG, March 1976), 104.
5. Q. C. Kessell and E. Everhart, Phys. Rev. 146 (1966), 16.
6. V. V. Afrosimov, Yu S. Gordeev, M. M. Panov, and N. V. Fedorenko, Sov. Phys.-Tech. Phys. 9 (1965), 1248; 9 (1965), 1256; 9 (1965), 1265.
7. U. Fano and W. Lichten, Phys. Rev. Lett. 14 (1965), 627.
8. M. Barat and W. Lichten, Phys. Rev. A 6, #1 (1972), 211.
9. J. S. Briggs and J. Macek, J. Phys. B 5 (1972), 579.
10. F. P. Larkins, J. Phys. B 5 (1972), 571. Also see J. D. Garcia, R. J. Fortner, and T. M. Kavanagh, Revs. Mod. Phys. 45 (1973), 111; P. Richard, "Ion Atom Collisions", in Atomic Inner-Shell Processes, ed. by B. Crasemann (Academic Press, 1975), 74-159.

11. K. Taulbjerg, J. S. Briggs, J. Vaaben, J. Phys. B 9, #8 (1976), 1351.
12. R. R. Randall, J. A. Bednar, B. Curnutte, C. L. Cocke, Phys. Rev. A 13, #1 (1976), 204.
13. R. R. Randall, Impact Parameter Dependence of Inner-Shell Vacancy Production in Fast Ion-Atom Collisions, Unpublished Doctoral Dissertation, Kansas State University, Manhattan, Kansas, 1975.
14. M. R. C. McDowell and J. P. Coleman, Introduction to the Theory of Ion-Atom Collisions (North-Holland Pub. Co., 1970), Chapter 4, "Impact Parameter Methods".
15. B. Fastrup, G. Hermann, Q. Kessel, and A. Crone, Phys. Rev. A 9, #6 (1974), 2518.
16. Q. C. Kessel and B. Fastrup, Case Studies in Atomic Physics, 3 (1973), 137-213.
17. D. R. Bates and D. A. Williams, Proc. Phys. Soc. 83 (1964), 425. Note that this formalism is similar to a simpler, restricted case, the Landau-Zener Model proposed in C. Zener, Proc. Royal Soc. A137 (1931), 696.
18. Some authors refer to this as Coriolis Coupling.
19. J. S. Briggs and J. Macek, J. Phys. B. 6 (1973), 982.
20. K. Taulbjerg and J. S. Briggs, J. Phys. B. 8, #11 (1975), 1895.
21. J. S. Briggs and K. Taulbjerg, J. Phys. B. 8, #11 (1975), 1909.
22. N. Bohr, Kgl. Danske Videnskab. Selskab, Mat-fys. Medd. 18 (1948), 8.
23. E. Everhart, G. Stone, and R. J. Carbone, Phys. Rev. 99, #4 (1955), 1287.

24. H. J. Stein, Stoßparameterabhängigkeit der L-Schalen-Ionisation von Jod und Tellur beim Beschußdünner Te-Targets mit 18-46 MeV J- Ionen, Jül-799-NP (September 1971), Kernforschungsanlage Jülich GMBH.
25. C. L. Cocke, R. R. Randall, S. L. Varghese, and B. Curnutte, Phys. Rev. A 14, #6 (1976), 2026.
26. Reference 13, Appendix A.
27. S. S. Gershtein and V. D. Krivchenkov, Soviet Physics JETP 13, #5 (1961), 1044, Equation 45.
28. P. Sigmund and K. B. Winterbon, Nuclear Inst. and Methods 119 (1974), 541.

Appendix A

Computer Code Used to obtain the Screened-Coulomb Impact Parameters for the Collision

The computer code given in this appendix is used to obtain the screened-Coulomb impact parameter when the angle θ of the scattered projectile is known. The angle θ is measured from the experimental apparatus. If the scattering were completely Rutherford in character, the impact parameter b would be given for small θ by

$$b = \frac{Z_1 Z_2 e^2}{E\theta} \quad (1)$$

where Z_1 = atomic number of target atom (28 for Ni)
 Z_2 = atomic number of projectile atom (29 for Cu)
 e^2 = 1.44 MeV-Fermi
 θ = scattering angle in radians
 E = projectile energy in MeV

and thus b will be in Fermis. (Note that 1 Fermi = 10^{-5} Å = 10^{-13} CM).

However, since the interaction potential between target and projectile atoms is obviously more complicated than a simple Coulomb (single-charge) potential because of the many additional electrons, it is necessary to use a more realistic potential function to compute the impact parameter. The potential normally used was suggested by N. Bohr²² and is called a screened-Coulomb potential. It is usually written as

$$V(r) \approx \left(\frac{e^2}{r}\right) \exp\left(\frac{-r}{a}\right) \quad (2)$$

where

$$a = \frac{a_0}{[Z_1^{2/3} + Z_2^{2/3}]^{1/2}} \quad (3)$$

and $a_0 = .53$ Å, the Bohr radius for hydrogen. The impact parameters for this potential are calculated using the method of Everhart, Stone and Carbone.²³ This calculation is performed by the following computer code.

To use the code, all that is needed is to insert a data card after the \$ ENTRY command. The data card has a format of 5D16.10 for the variables:

A B ROA FLIM SLIM

A is the a given in expression (2) above. B is given by

$$B = \frac{z_1 z_2 [1.44 \times 10^{-5} \text{ MeV} - A]}{E} \quad (4)$$

where E is projectile energy in MeV. ROA was set equal to zero for these calculations. FLIM and SLIM are the lower and upper limits of integration, respectively; for these calculations FLIM = 10.0 and SLIM = 200.0 give sufficiently accurate results.

The program was checked for accuracy by reproducing the impact-parameter calculation of Stein²⁴ for Iodine on Tellurium at 18.6, 30.8, and 46 MeV before the computations for this thesis (Copper on Nickel) were performed.

ILLEGIBLE DOCUMENT

**THE FOLLOWING
DOCUMENT(S) IS OF
POOR LEGIBILITY IN
THE ORIGINAL**

**THIS IS THE BEST
COPY AVAILABLE**

\$J03

DOUBLE PRECISION F04,A,B,CK,PA,DSORT,DEXP,DELTA,SLOPE,THETAK,THETA
DOUBLE PRECISION DSIG,P,SIG4,FLIM,SLIM,DSIG1,DSIG2,RATIO

C THIS PROGRAM COMPUTES SCATTERING IMPACT PARAMETERS FOR AN EXPONENTIALLY-
C SCREENED COULOMB POTENTIAL. OTHER RELEVANT QUANTITIES ARE ALSO CALCULATED.
C
C THE METHOD AND NOTATION USED ARE FROM EVERHART, STONE, AND CARPONE,
C PHYSICAL REVIEW 99, 84 (AUGUST,1955),PAGE 1267.
C
C EQUATION (17) OF THIS PAPER IS INTEGRATED NUMERICALLY. IT IS BROKEN INTO TWO
C PARTS IN ORDER TO AVOID THE DIVERGENCE AT U=1.
C
C THIS PROGRAM WAS WRITTEN BY RUSSEL RANDALL IN 1974 AND MODIFIED SLIGHTLY BY
C CLARENCE ANNETT IN 1976.
C
C
C DEFINITION OF VARIABLES:
C A= SCREENING RADIUS, GIVEN BY EXPRESSION (2) IN EVERHART,ET AL.
C B= DISTANCE OF CLOSEST APPROACH IN A HEAD-ON COLLISION, GIVEN BY
C EXPRESSION (3) IN EVERHART, ETAL.
C ROA= B/A, WHERE B= DISTANCE OF CLOSEST APPROACH FOR THE PARTICULAR
C IMPACT PARAMETER.
C F= SCREENED COULOMB IMPACT PARAMETER
C BRUTH = RUTHERFORD IMPACT PARAMETER =B/THETA.
C THETA= THE LAB SCATTERING ANGLE, IN RADIAN.
C THETAK=THETA*A/E, AS PER EXPRESSION (17).
C THETA4*SIGMA= THETA TO THE 4TH POWER TIMES THE TRUE SCATTERING CROSS
C SECTION. IF THIS IS CONSTANT, THE SCATTERING IS RUTHERFORD.
C SIGMA RATIO= RATIO OF SCREENED-COULOMB SCATTERING CROSS SECTION TO
C RUTHERFORD SCATTERING CROSS SECTION, FOR THIS LAB ANGLE THETA.
C
C THE UNITS ARE CONSISTENT WITHIN THE PROGRAM; IF A AND B ARE INPUT IN
C ANGSTROMS, THE P AND BRUTH WILL BE IN ANGSTROMS ALSO.

READ (5,1) A,B,ROA,FLIM,SLIM
1 FORMAT (5F16.10)
WRITE(6,4)A,B
4 FORMAT(1H0,'SCREENEDING RADIUS= ',D20.9,'CLOSEST APPROACH ',D20.
C9)
WRITE (6,12)
12 FORMAT (/26H THE UNITS ARE ANGSTROMS. /)
WRITE(6,2)
2 FORMAT(1H1,9X,'ROA LIST',15X,'P LIST',14X,'THETA LIST',14X,'THETAK
C',11X,'THETA4*SIGMA LIST',7X,'SIGMA RATIO')
5 CONTINUE
ROA=ROA+.25D-1
CK=A/F
PA=DSORT*(ROA=ROA-(1.0D0)/CK)*ROA*DEXP(-ROA)
DELTA= SQRT((ROA+.5D-2)**2.0D0-(1.0D0/CK)*(ROA+.5D-2)*DEXP(-(ROA+
C.5D-2)))
DELTA= DELTA-DSORT((ROA-.5D-2)**2.0D0-(1.0D0/CK)*(ROA-.5D-2)*DEXP(
C-(ROA-.5D-2)))
DSIG1=DSIG(1.0D0,FLIM,ROA+.5D-2)+DSIG(FLIM,SLIM,ROA+.5D-2)
DSIG2=DSIG(1.0D0,FLIM,ROA-.5D-2)+DSIG(FLIM,SLIM,ROA-.5D-2)
SLOPE=(DSIG1-DSIG2)/DELTA
THETAK=DSIG(1.0D0,FLIM,ROA)+DSIG(FLIM,SLIM,ROA)
SIG4=(-PA/SLOPE)*((A/CK)**2)*(THETAK**3)
RATIO=SIG4*(CK/A)**2.0D0
THETA=THETAK/CK

```

P=PA*A
WRITE(6,3)ROA,P,THETA,THETAK,SIG4,RATIO
3 FORMAT(1H,C,6(D20.10,2X))
BRUTH=P/THETA
WRITE(6,10)BRUTH
10 FORMAT(1H,' RUTHERFORD B=',F8.5)
IF (ROA.GE.4.0000) GO TO 6
GO TO 5
6 CONTINUE
CONTINUE
STOP
END

C
C THIS ROUTINE CALCULATES DOUBLE INTEGRALS BY ROMBERG METHOD
DOUBLE PRECISION FUNCTION DSIG(C,D,ROA)
DOUBLE PRECISION POA
DOUBLE PRECISION QUAD(10,10),A,B,C,D,Y,FACTOR
DOUBLE PRECISION HALF,CNE,TWO,FOUR
REAL*8 GNT
DOUBLE PRECISION DABS
FACTOR=1.000
4001 FORMAT(1H,C,' ACCURACY WAS NOT OBTAINED FOR THE NEXT VALUES')
CNE=1.000
HALF=.5000
TWO=2.000
FOUR=4.000
ERROR=.00001
JMAX=15
QUAD(1,1)=((D-C)/TWO)*(GNT(C,ROA)+GNT(D,ROA))
DO 2 K=2,JMAX
Y=(D-C)/TWO*(K-1)
QUAD(1,K)=HALF*QUAD(1,K-1)
L=(2*(K-1))-1
DO 1 I=1,L,2
QUAD(1,K)=QUAD(1,K)+Y*GNT((I*Y)+C,ROA)
1 CONTINUE
DO 3 N=2,K
QUAD(N,K-N+1)=(CNE/(FOUR*(N-1)-CNE))*(((FOUR*(N-1))*
2(QUAD(N-1,K-N+2))-QUAD(N-1,K-N+1))
IF(DABS((QUAD(N,K-N+1)-QUAD(N-1,K-N+2))/QUAD(N,K-N+1)).LT. ERROR)
2GO TO 4
3 CONTINUE
2 CONTINUE
WRITE(6,4001)
GO TO 5
4 CRST=QUAD(N,K-N+1)*FACTOR
DSIG=CRST
5 RETURN
END
DOUBLE PRECISION FUNCTION GNT(Y,ROA)
DOUBLE PRECISION X,Y
DOUBLE PRECISION DEXP
DOUBLE PRECISION DSQRT
DOUBLE PRECISION ROA
GNT=((ROA)*DSQRT(Y*Y-1.000))/DEXP(ROA*Y)
RETURN
END
$ENTRY

```

Appendix B

Coupled-Channel Computer Code

This appendix contains a computer code which solves the coupled-channel equations (13) and (14) of Section II, as derived by Briggs and Macek⁹. The impact-parameter dependent probability curves calculated by Taulbjerg, et.al.¹¹ can be reproduced by this program, although agreement is not exact because the method used by Taulbjerg, et al. is more refined. The scaling law given by Taulbjerg, et al. is included in the program; no further scaling of the results is necessary.

To use the program, a data card of format (7F10.0, I5) is placed after the \$ ENTRY command. The data card contains the following information:

B DB E ZS A RO DT N

where B = the initial (smallest) impact parameter in atomic units

DB = the impact parameter increasment

E = the projectile energy in MeV

ZS = the effective nuclear charge of the target atom

A = the atomic mass of the projectile atom

RO = .2

DT = the time increasement in atomic units (.2 works well)

N = 10

The impact parameter b is printed out in Angstroms.

```

$JCB      ,TIME=(,10)
C
C      COUPLED STATE PROGRAM
C      THIS PROGRAM IS A SIMPLIFIED METHOD OF SOLVING THE COUPLED CHANNEL
C      EQUATIONS GIVEN IN PRIGGS AND MACEK TO OBTAIN THE IMPACT-PARAMETER
C      DEPENDENT PROBABILITY CURVES GIVEN IN TAULBJERGS THIRD PAPER. THE
C      PROGRAM INCLUDES THE PROPER SCALING AS DEMANDED BY TAULBJERG.
C
C      THIS PROGRAM WAS WRITTEN BY C. L. COCKE AND MODIFIED BY CLARENCE
C      ANNETT IN 1976.
C
C      PROGRAM DOES CALCULATIONS IN AU
C      B IS IMPACT PARAMETER IN AU
C      WILL DO N CASES FOR B IN INCREMENTS OF DB
C      WRITES B IN ANGSTROMS
C      E IS ENERGY OF PROJECTILE IN MEV
C      ZS IS EFFECTIVE NUCLEAR CHARGE FOR SYMMETRIC CASE
C      ZS SQUARED IS ALSO EFFECTIVE Q SQUARED FOR PROJECTILE PATH
C      A IS PROJECTILE MASS IN AMU
C      DT IS TIME INCREMENT IN AU. PROGRAM SCALES THIS BY ZS**2,SO TRY
C      SETTING DT=1.0 IF IN DOUBT
C      INTEGRATES FROM R0(AU) IN AND OUT TO R0 AGAIN
C      IF NOT SYMMETRIC COLLISION, TAKE ZS=SQRT(Z1*Z2)
C      PROGRAM PRINTS OUT RESULTS AT HALF AND FULL PASS,IN THAT ORDER
C
      NR=5
      NW=6
6      READ(NR,1) B,DB,E,ZS,A,R0,DT,N
      WRITE (6,25)
25      FORMAT (1F1)
      WRITE (6,27)
27      FORMAT (25H 65 MEV COPPER ON NICKEL //)
      WRITE(NW,50)
50      FORMAT(' H12(AU)      E(MEV)      ZS      A(AMU)      R(AU)      P
X          DELTA E      P1  ' //)
      SUM=0.0
      RF=R0+.001
      V=SQRT(E/(A*.025))
1      FORMAT(7F10.0,15)
      DT=DT/(ZS*ZS)
      DO 7 J=1,N
      BB=8*.53
      WRITE(NW,51) DT,BB
51      FORMAT(' DT=',F10.5,' B(A) =',F10.5)
C
C      INITIALIZE PARAMETERS
      ICT=0
      A1=1.0
      A2=0.0
      A3=0.0
      A4=0.0
      EP=0.0
      R=R0
      ITEST=0
C
C      CALCULATE CHANGING PARAMETERS
3      Z=(V*V*(1.-(B*B)/(R*R))-1.0*ZS*ZS/(460.*R*A))
      IF (Z.GE.0.) GO TO 4
      ITEST=1
      Z=-Z

```

```

      WRITE(NW,5)CH12,E,ZS,A,R,P,Z,P2
4     PDOT=SGRT(Z)
C     ALP IS DT* COUPLING HAMILTONIAN IN AU
C     ROTATIONAL COUPLING H
      ALP=((DT*B*V)/(R*R))*EXP(-(ZS*ZS*R*R)/16.)
      CH12=ALP/DT
      C=CCS(EP)
      S=SIN(EP)

C
C     INCREMENT EVERYTHING
C     Z HERE IS ENERGY SEPARATION OF COUPLED STATES IN AU
C     THESE TWO STATEMENTS DETERMINE THE ENERGY SEPARATION OF THE 2PPI
C     AND THE 2PSIGMA LEVELS.
      Z=.375*(1.-EXP((1.6-R*ZS)/1.4))
      IF (Z.LE.0.093) Z=.093*R*R*ZS*ZS

C
      Z=Z*ZS*ZS
      EP=EP+DT*Z

C
C     FOR REAL COUPLING HAMILTONIAN
      A4=A4+ALP*(-A1*C-A2*S)
      A3=A3-ALP*(-A2*C+A1*S)
      A2=A2-ALP*( A3*C-A4*S)
      A1=A1+ALP*( A4*C+A3*S)
      P1=A1+A1+A2*A2
      P2=A3*A3+A4*A4
      P=P1+P2
      R=R-REGT*DT*(-1.0)**ITEST
5     FORMAT(8F10.5)
      ICT=ICT+1
      X=ICT/10
      ICTT=X*10.
52    IF(R.LE.RF) GO TO 3
      WRITE(NW,5)CH12,E,ZS,A,R,P,Z,P2
      SUM=SUM+PB*P1*2.*3.1416*CB*.53
7     B=B+CB
      WRITE(NW,60) SUM
60    FORMAT(' SIGMA(SQANG)=' ,1PE12.5)
      WRITE (6,25)
      GO TO 6
      END
$ENTRY

```


APPENDIX C

Conversion of X-ray Production Probability to K-Vacancy Production Probability

Under the presumption that the rotational coupling process is operating, the measured nickel K_{α} x-ray production probability $P_x(b)$ of Figures 8 and 9 may be converted to a $2p\sigma$ vacancy production probability $P_{2p\sigma}(b)$.

Begin with the expression

$$P_x(b) = N_{2p\pi} P_{ROT}(b) W \omega_{NiK\alpha} \quad (3)$$

where $N_{2p\pi}$ = number of $2p\pi$ vacancies brought into the inner region of the collision by the copper beam,

$P_{ROT}(b)$ = the probability for $2p\pi$ - $2p\sigma$ rotational coupling to occur, as a function of impact parameter,

$\omega_{NiK\alpha}$ = the K_{α} fluorescence yield for nickel,

W = the fraction of nickel K-vacancies to total (nickel plus copper) K-vacancies.

Note that

$$W \approx \frac{\# \text{ nickel K x-rays}}{\# \text{ total K x-rays}} \quad (4)$$

$$= \left[\frac{\# \text{ nickel } K_{\alpha} \text{ x-rays}}{\# \text{ total K x-rays}} \right] \left[\frac{K}{K_{\alpha}} \right] \quad (5)$$

where $\frac{K}{K_{\alpha}}$ = the ratio of nickel K X rays to nickel K_{α} X rays.

Also,

$$\omega_{NiK\alpha} = \omega_K \left[\frac{K_{\alpha}}{K} \right] \quad (6)$$

where $\omega_K = 0.414$, the K-shell fluorescence yield for nickel;
and

$$P_{2p\sigma}(b) = [N_{2p\pi} P_{ROT}(b)] \quad (7)$$

Combining equations (3) through (7), we obtain

$$P_{2p\sigma}(b) = \frac{P_X(b)}{f_{Ni} \omega_K} \quad (8)$$

where f_{Ni} is the fraction of nickel K_α x-rays/total Copper plus Nickel K X rays observed in coincidence runs. This fraction was found to have the value 0.49 for 50 MeV runs and 0.52 for 65.6 MeV runs, and is independent of impact parameter.

The number of $2p\pi$ vacancies brought into the collision by the copper beam, $N_{2p\pi}$, can now be estimated. If P_{ROT}^{MAX} is the maximum value of $P_{2p\sigma}$ given by Taubjerg's calculations¹¹ and $P_{2p\sigma}^{MAX}$ is the maximum K_α x-ray production probability observed, then

$$P_{2p\sigma}^{MAX} = P_{ROT}^{MAX} N_{2p\pi} \quad (9)$$

$$= \frac{n_{2pcu}}{6} P_{ROT}^{MAX} \quad (10)$$

where n_{2pcu} is the average number of 2P vacancies brought in by the copper beam. Figures 8 and 9 give the result that at 50 MeV, two vacancies are brought in by the beam; and at 65.6 MeV, 3.6 vacancies are brought in by the beam. However, these numbers are dependent on the thickness of the

target. If these values are extrapolated to zero target thickness using Figure 13, they become 0.89 vacancy for 50 MeV and 1.59 vacancies for 65.6 MeV. The saturation values, for an infinitely thick target, are 2.44 vacancies for 50 MeV and 4.36 vacancies for 65.6 MeV.

IMPACT PARAMETER DEPENDENCE
OF K-VACANCY PRODUCTION IN
COPPER-NICKEL COLLISIONS AT 50 AND 65.6 MeV

by

Clarence Howard Annett
B. S., Texas A. & M. University, 1975

An Abstract of
A Master's Thesis

Submitted in partial fulfillment of the
requirements for the degree

MASTER OF SCIENCE

Department of Physics
Kansas State University
Manhattan, Kansas

1977

Abstract

Collisions between copper ions and thin, solid nickel targets at 50 and 65.6 MeV are observed. The nickel K_{α} x-ray production probability per particle is measured as a function of the impact parameter using scattered particle x-ray coincidence techniques. The resulting probability is a direct measure of the nickel K-vacancy production probability. Solid target effects and small-angle scattering are considered.

The data is compared to calculations¹ using a molecular-orbital (MO) model for atomic collisions, assuming $2p\sigma$ - $2p\pi$ rotational coupling. Some disagreement between theory and experiment is noted, and an attempt is made to correct the model to agree with experimental results.

¹K. Taulbjerg, J. S. Briggs, and J. Vaaben, J. Phys. B 9, #8 (1976), 1351.